

University of Montana

## ScholarWorks at University of Montana

---

Graduate Student Theses, Dissertations, &  
Professional Papers

Graduate School

---

2022

# DERIVING SURFACE FUELS FROM UAS IMAGERY FOR FIRE MODELS

Matthew R. Cunningham  
*University of Montana, Missoula*

Follow this and additional works at: <https://scholarworks.umt.edu/etd>



Part of the [Forest Management Commons](#)

## Let us know how access to this document benefits you.

---

### Recommended Citation

Cunningham, Matthew R., "DERIVING SURFACE FUELS FROM UAS IMAGERY FOR FIRE MODELS" (2022).  
*Graduate Student Theses, Dissertations, & Professional Papers*. 11874.  
<https://scholarworks.umt.edu/etd/11874>

This Thesis is brought to you for free and open access by the Graduate School at ScholarWorks at University of Montana. It has been accepted for inclusion in Graduate Student Theses, Dissertations, & Professional Papers by an authorized administrator of ScholarWorks at University of Montana. For more information, please contact [scholarworks@mso.umt.edu](mailto:scholarworks@mso.umt.edu).

DERIVING SURFACE FUELS FROM UAS IMAGERY FOR FIRE MODELS

By

Matthew Ryan Cunningham

Bachelor of Arts, University of Montana, Missoula, Montana, 2013

Thesis

presented in partial fulfillment of the requirements  
for the degree of

Master of Science  
in Forestry

The University of Montana  
Missoula, MT

May 2022

Approved by:

Scott Whittenburg, Dean of The Graduate School  
Graduate School

Carl Seielstad  
Department of Forestry

Lloyd Queen  
Department of Forestry

Charles Palmer  
School of Integrative Physiology and Athletic Training

## DERIVING SURFACE FUELS FROM UAS IMAGERY FOR FIRE MODELS

Understanding how fuel, weather, and terrain interact to produce fire behavior continues to motivate fire science and has resulted in development of new physics-based fire behavior models that place increased demands on input data such as fuels. Recent technological advancements in computing, unmanned aerial systems (UAS), and sensors (RGB, multispectral, thermal, and hyperspectral cameras) can provide new opportunities for land managers and scientists to advance knowledge of fuels and fire behavior and their interactions on the landscape. In this study, imagery from high resolution multispectral cameras mounted on UAS were used to build orthomosaics and point clouds of surface fuelbeds in grass, litter, and shrub fuels of the Sycan Marsh Preserve in Oregon. The purpose of this effort was to develop useful inputs to a fuels translator called STANDFIRE that prepares fuels data for use in physics-based fire models. Fuel type polygons were delineated using traditional photo-interpretation for nine 1 ha plots that were ultimately treated with fire. Each fuel polygon was attributed from field-collected data based on their dominant fuel type. Differences between fuel type polygons were assessed statistically to document the distinctiveness of each fuel type, to overcome field sample-size limitations, and to provide logic for merging fuel types that were similar. Additionally, 3D point clouds and orthomosaics were examined to better understand their information content for more detailed characterizations of fuels. In this latter part of the research, shrub height, width, and cover were extracted from the point clouds and compared to field measurements. The findings were as follows: Defensible fuel type classes were easily delineated using photo-interpretation, resulting in 21.4% of the cumulative plot area classified as litter, 65.3% as grass and 10.3% as shrub fuels. Effective attribution of fuel polygons was dependent on how and where field data were collected and differed by year. Lack of sufficient sample sizes in some fuel type polygons required aggregation of field data from all plots within the Brattain burn unit in 2018. These shortcomings were overcome in 2019 by acquiring rapid-look imagery prior to field sampling that enabled more balanced samples across the range of variability, along with utilization of precision GPS. Within the point-clouds, shrub height was underestimated while width was over-estimated. Shrub cover was also under-predicted from the point cloud and was better enumerated using a conventional dot-grid approach on the orthomosaic. Improvements in data collection methods from 2017-2019 have resulted in a stable workflow that produces consistent fuels data formatted for STANDFIRE. The polygon-based approach is suitable for use in fire model validation due to its ability to rationally integrate sparse field data, because STANDFIRE is designed to work easily with polygons, and because there is insufficient evidence that model validation is at a point where it will benefit from use of more complex pixel or object-based inputs. Automated approaches to polygon delineation via region-growing, machine learning, and segmentation are a logical next step, with the caveat that the inputs derived in this study should be tested in the modeling environment first.

## Contents

1. Introduction.....	- 1 -
1.1 Overview.....	- 1 -
1.2 Objectives .....	- 4 -
2. Methods .....	- 6 -
2.1 Study Area .....	- 6 -
2.2 Data Collection and Processing .....	- 10 -
2.3 Derive Fuel-type Polygons using Photointerpretation .....	- 21 -
2.4 Attribute Fuel Polygons from Field Measurements .....	- 24 -
2.5 Quantify and Compare Shrub Heights and Widths.....	- 29 -
2.6 Derive a ground surface for generation of the CHM .....	- 30 -
3. Results.....	- 34 -
3.1 Derive Fuel-type Polygons using Photointerpretation .....	- 34 -
3.2 Attribute Fuel Polygons from Field Measurements .....	- 35 -
3.3 Quantify and Compare Shrub Heights and Widths.....	- 45 -
3.4 Assess Shrub Cover Derived from UAS Point Clouds .....	- 46 -
4. Discussion.....	- 49 -
4.1 Objective 1. Derive Fuel-type Polygons using Photointerpretation.....	- 49 -
4.2 Objective 2. Attribute Fuel Polygons from Field Measurements.....	- 50 -
4.3 Objective 3. Quantify and Compare Shrub Heights and Widths .....	- 51 -
4.4 Objective 4. Assess Shrub Cover Derived from UAS Point Clouds.....	- 52 -
4.5 Data Collection and Data Quality .....	- 54 -
5. Conclusions.....	- 55 -
6. References Cited.....	- 58 -
7. Appendices.....	- 62 -
7.1 Appendix A.....	- 62 -
7.2 Appendix B .....	63
7.3 Appendix C .....	65

Figure 1. Sycan Marsh Preserve Study Area and plots .....	- 6 -
Figure 2. 2017 painted numbered GCP, 2018 GCP polished steel plate and 2019 GCP .....	- 10 -
Figure 3. DJI M100 quadcopter .....	- 12 -
Figure 4. Map Pilot's Pro Business Edition flight plan .....	- 13 -
Figure 5. Micasense calibration panels bands 1-5 .....	- 14 -
Figure 6. 1m <sup>2</sup> square photoload sample plot .....	- 15 -
Figure 7. Hula-Hoop photoload sample plot.....	- 16 -
Figure 8. Agisoft Metashape processing.....	- 17 -
Figure 9. Brattain H topology rule used to correct polygons.....	- 24 -
Figure 10. Sample photo-load used for field data.....	- 26 -
Figure 11. Example of fishnet plot used to estimate shrub cover .....	- 27 -
Figure 12. Rasterized shrub heights Brattain H .....	- 29 -
Figure 13. Random points for shrub measurements.....	- 30 -
Figure 14. Smoothing the DSM output from Metashape.....	- 32 -
Figure 15. Brattain H delineated fuel polygons .....	- 34 -
Figure 17. Overhead image to aid sampling .....	- 38 -
Figure 19. Ten random points for shrub measurements.....	- 45 -
Figure 26. Segmentation fuel classification based on principle component analysis .....	- 50 -
Boxplot 1. 2018 grass cover by fuel type.....	- 37 -
Boxplot 2. 2018 grass load by fuel type.....	- 37 -
Boxplot 3. 2018 litter depth by fuel type .....	- 37 -
Boxplot 4. 2018 gras height by fuel type .....	- 37 -
Boxplot 5. 2018 litter cover by fuel type .....	- 38 -
Boxplot 6. 2018 shrub cover by fuel type.....	- 38 -
Boxplot 7. 2019 shrub cover vs. plot .....	- 42 -
Boxplot 8. 2019 grass load vs. plots .....	- 42 -
Boxplot 9. 2019 litter depth vs. plots.....	- 43 -
Boxplot 10. 2019-hundred-hour fuel vs. plots .....	- 43 -
Boxplot 11. 2019 Ten-hour fuel vs. plot.....	- 43 -
Boxplot 12. 2019 One-hour fuel vs. plot .....	- 43 -
Boxplot 13. 2019 grass cover vs. fuel type.....	- 44 -
Boxplot 14. 2019 grass height vs fuel type.....	- 44 -
Boxplot 15. 2019 grass load vs. fuel type .....	- 44 -
Boxplot 16. 2019 grass height vs. fuel type.....	- 44 -
Boxplot 17. Modeled vs. field measured shrub heights.....	- 46 -
Boxplot 18. Modeled vs. field measured shrub widths.....	- 46 -
Table 1. Plots used in this analysis .....	- 8 -
Table 2. Photo-interpretation key.....	- 22 -
Table 3. 2018 Fuel samples summary.....	- 36 -
Table 4. 2019 fuel sample summary .....	- 39 -
Table 5. Fishnet derived shrub cover .....	- 47 -
Table 6. CHM derived shrub cover.....	- 48 -

# 1. Introduction

## 1.1 Overview

As wildfires continue to occur and the encroachment of the wildland urban interface (WUI) continues to develop at unprecedented rates across the West (Calkin, Cohen et al. 2014, Radeloff, Helmers et al. 2018), land managers face a complex task of managing landscapes and balancing growing public and commercial interests in and around public lands. The focus of fire management in recent years has shifted from suppression as the main objective to include fire as a natural process (Young, Evans et al. 2020) that is needed on the landscape to help restore our forests to what they once were before suppression (Cleaves, Haines et al. 1999, Kolden 2019). Restoring the role of fire in turn places new demands on science and technology to inform when, where, and how we use fire for the benefit of ecological objectives. Quantifying surface fuels in forests is problematic for land managers due to the difficulty in measuring fuels of different sizes, strata, and spatial variability, yet surface fuels play a key role in fire behavior and fire spread (Ottmar, Sandberg et al. 2007). Current approaches of classifying surface fuels can be time intensive, costly, and are often not practical to cover large areas. New technological advancements in computing and unmanned aerial systems (UAS) and sensors (red, green, blue multispectral, thermal, and hyperspectral cameras) can provide new opportunities for land managers and scientists to advance knowledge of fire behavior and its interactions on the landscape (Hoffman, Sieg et al. 2018).

In June of 2016 the Federal Aviation Administration (FAA) introduced a new rule for UAS, Part 107 (FAR/AIM 2016). This new law codified the commercial use of UAS within the National

Airspace (NAS) in the United States (US). After this rule was introduced their commercial and research-based uses have greatly expanded since 2016 (Canis 2015). UAS provides new and novel ways to collect high resolution visible, thermal, hyperspectral, and multispectral data that were not economical or possible on a large scale until recent years without the use of a manned aircraft (Patrick, Temuulen et al. 2018, Moran, Seielstad et al. 2019). Additionally, technological advancements in computing capacity have allowed new computational fluid dynamics (CFD) fire behavior modeling systems to advance (Mell, Jenkins et al. 2007, McGrattan, McDermott et al. 2012, Mell, Charney et al. 2013), yet at the same time these emerging models have distinct needs for more complex fuels data, more specifically surface fuels (Bradshaw 1986, Linn, Goodrick et al. 2020) which are the primary drivers of fire and fire behavior in wildland fire.

Two of the commonly used CFD fire behavior models are FIRETEC and Wildland-Urban Interface Dynamics Simulator (WFDS). FIRETEC was developed at the Los Alamos National Laboratory (LANL) from military models used to predict dispersion of chemical and biological agents released on the battlefield landscape (Hanson, Bradley et al. 2000). This physics based CFD model uses many of the same inputs that are also crucial factors in wildfire modeling. The downside to FIRETEC is that it is very computationally intensive and in its current state is only available to researchers at the Los Alamos National Lab. The second more accessible physics based CFD model is Wildland Fire Dynamic Simulator (WFDS). WFDS was developed in collaboration with the National Institute of Standards and Technology (NIST) and the Fire Dynamic Simulator (FDS) (McGrattan and National Institute of Standards, 2000). The main goal of FDS was to use physics based CFD modeling to simulate structure fires and their interactions with materials and wind fields within and around the main structure. WFDS evolved from FDS as the FDS model was incorporated into the wildland-urban environment (WUI) to simulate how

fire moved from fuels outside the structure to the structures themselves (Meerpoel-Pietri, Tihay-Felicelli et al. 2022).

CFD model requirements for detailed fuels and weather information are intense and inputting fuels into the models is complex, cumbersome and time consuming (Prichard, Keane et al. 2017). These limitations have led to the development of a fuel translator called STANDFIRE (Pimont, Parsons et al. 2016). STANDFIRE takes spatially explicit fuel information and converts it into a text file (Appendix A) that can be consumed by FIRETEC and WFDS. STANDFIRE reads outputs from Fire and Fuels Extension (FFE) and Forest Vegetation Simulator (FVS) (Reinhardt 2003, Crookston and Dixon 2005) using a fire library to convert them to 3D fuels. These approaches have their downsides as well as pitfalls and are not non-scientist friendly (Noonan-Wright, Vaillant et al. 2014). Within the STANDFIRE framework, fuels can be modeled as objects (plants) or as layerSets (layers/areas with known fuel characteristics). These fuel types can be mixed in fire simulations and changed based on what is exhibited on the ground.

The focus of this thesis will be on developing layerSets describing surface fuel characteristics from UAS imagery. STANDFIRE creates a text file, within that text file, vertices are created that define fuel polygons (Appendix B). Each fuel polygon is given metrics based on sampled fuels within that plot. STANDFIRE incorporates three different fuel types: shrub, herbaceous and litter. There can be all three fuel types (shrub, litter, and herbaceous) within a single polygon. Each fuel type that is represented in the polygons is given a height, base height, cover (fraction), patch size, and an integer code identifying it to a spatial group. Live and dead fuels are attributed with bulk density, particle density, surface area to volume ratio (SAV), and moisture content as a percent. From these inputs, STANDFIRE generates spatially explicit fuels that maintain the properties of the inputs, like FFE-FVS.



This project seeks to develop methods to classify surface fuels from high resolution UAS derived imagery for use in CFD fire behavior modeling, specifically through the new fuel translator STANDFIRE (Pimont, Parsons et al. 2016). This is part of a larger project to collect integrated weather, fuels, topography, and fire behavior datasets for model validation. Logically, outputs from these models will allow managers to assess alternative strategies to meet their ecological objectives or management objectives (Linn, Goodrick et al. 2020). Thus, modelers, managers and practitioners need access to current, high resolution fuels data. The overarching goal of the project is to produce rational, spatially explicit surface fuels data for direct input into STANDFIRE and to develop a repeatable workflow that allows a capable but non-scientific individual (e.g., fire manager/land manager) to input fuels data into a CFD model easily. This research also informs the development of STANDFIRE itself.

The outcome of this thesis is fuels data for use in a collaborative effort between multiple state, federal, and private agencies to study prescribed fire and model its effects on pre, during and post burn fire processes. Some of the methods used were the result of other experimental needs within this collaborative effort.

## **1.2 Objectives**

This thesis will address the following four objectives.

1. Derive fuel-type polygons using traditional photointerpretation to mimic a fire manager's approach to fuels classification.
2. Attribute fuel polygons from field measurements and compare fuel attributes across fuel types.

3. Quantify and compare shrub heights and widths based on field vs. point-cloud modeled and measurements.
4. Assess shrub cover derived from UAS point cloud height classification, field measurements, and conventional point-intercept (dot-grid) and compare across fuel types and against field measurements.

The organization of this thesis is a traditional Introduction, Methods, Results, Discussion, Conclusions. Each of the following sections is organized specifically around the four objectives identified above. In addition, because a major part of this thesis was data collection and processing using UAS and I was a major contributor in terms of time, effort, and intellectual engagement, data collection procedures are described in detail in the methods section below.

# 2. Methods

## 2.1 Study Area

Throughout a three-year timeframe (2017-2019), twenty-three (Figure. 1) 100 x 100m plots were installed across three burn units that spanned open tall grass, short grass, western bunchgrass,

### Sycan Research Units

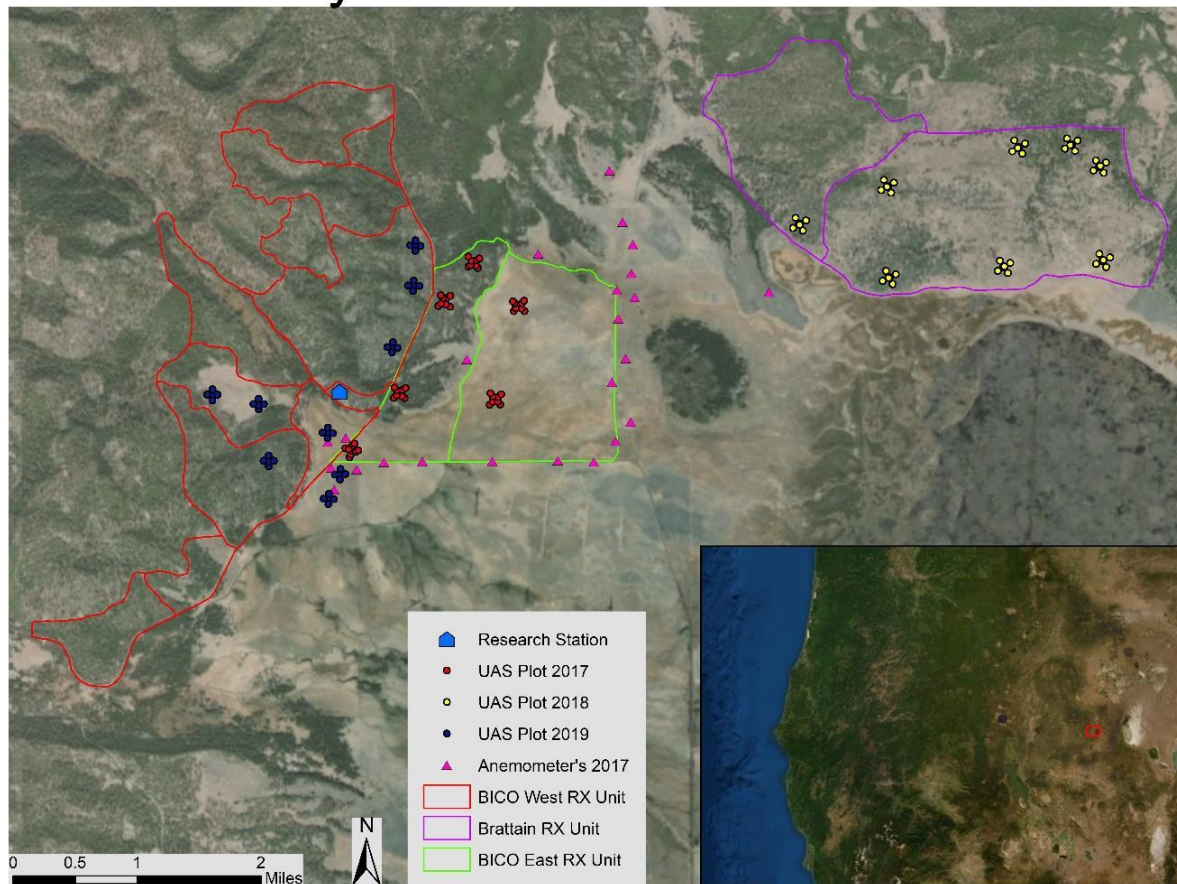


*Figure 1. Sycan Marsh Preserve Study Area and plots*

ponderosa pine forest, and sage-bitterbrush flats in Sycan Marsh Preserve, OR. The twenty-three units incorporated all the landscapes and fuel types that are present on the preserve lands at this location. Of the twenty-three total plots, nine (Table. 1) are used in this thesis, all from 2018 and 2019. This is because some plots did not contain complete data or did not experience useful fire

behavior, were never burned due to environmental considerations or fire reached the plots before during fire behavior imagery could be taken which was part of the collaborative effort to study fire behavior.

Sycan Marsh is in the Klamath Basin, in Lake County, Oregon. The land is owned and managed by the Oregon chapter of The Nature Conservancy (TNC) and is surrounded by the Fremont-Winema National Forest and private inholdings. The name Sycan is derived from the Klamath Native American term "saiga keni" and the name Sycan means "level, grassy place" (The Nature Conservancy 2020). The dominant fuel types within this area are open ponderosa pine with litter, grass, shrubs, western bunchgrasses, marsh grasses, and xeric shrublands. The area is characterized by a high desert climate with hot dry summers and cold dry winters, the average annual high temperature is 64F, while the average low is 30F (U.S. Climate Data 2020). The area receives an average of 10.3 inches of precipitation annually and experiences an average of 23 inches of snowfall per year (U.S. Climate Data 2020).

Plot	Year	Burn Unit	Sensor
Brattain_B	2018	Brattain	X3/MSRE
Brattain_C	2018	Brattain	X3/MSRE
Brattain_F	2018	Brattain	X3/MSRE
Brattain_H	2018	Brattain	X3/MSRE
1A_Grass	2019	BICO West	X3/MSRE
1C_Grass	2019	BICO West	X3/MSRE
1C_Forest	2019	BICO West	X3/MSRE
Southern_Grass_1	2019	BICO West	X3/MSRE
Southern_Grass_2	2019	BICO West	X3/MSRE
X3 – DJI Zemuse X3 12MP			
MSRE – Micasense Rededge Multispectral camera.			

*Table 1. Plots used in this analysis*

The overall approach to this project was to image 100 x 100 m plots within burn units using optical sensors mounted on UAS, derive fuel type polygons within each plot, attribute these polygons with field measurements of fuels, and create STANDFIRE inputs for each fuel type (Objectives 1 and 2). In order to achieve these ends, it was necessary to analyze similarities and differences in fuel attributes among fuel types, in part to overcome sample size limitations, and these analyses were used to justify aggregation of field plot data for some fuel type polygons. Additionally, the point clouds were examined to better understand how fuel objects such as shrubs were dimensioned and how they could be used to estimate STANDFIRE attributes such as shrub cover and patch size. The latter two areas of investigation (Objectives 3 and 4) were

intended to begin identifying strengths and limitations of point clouds derived from imagery as a source of information for fine-scale fuels mapping.

The project utilized data collected in 2018 and 2019, including eight plots in 2018 and nine in 2019. The first two objectives applied to data in both years, while the second two objectives utilized only data from the Brattain burn unit because this was where shrubs measured in the field coincided with high-quality remote sensing data and successful end-to-end (pre-, during, -post-fire) data collections. Due to the nature of method development in the larger project the methods to collect data also evolved from one year to the next resulting in some different issues and approaches in each year. For example, in 2018, field measurements were not explicitly aligned with fuel type polygons because the polygon approach was not adopted until after evaluating the data. As a consequence, there were sample size limitations on field data for some fuel types that required logic for aggregating field data from other plots. Additionally, field plots in 2018 were not well-located due to limits in GPS technology combined with field methodology, and thus it was necessary to validate and attribute by polygon rather than pixel or object. Both of these issues were addressed in 2019 by acquiring rapid-look imagery pre- field data collection, locating plots within areas of similar tone/texture/color (e.g., fuel type polygons), and collecting the location of each field measurement with a newly acquired pair of dual-frequency, kinematic GPS receivers in a rover-base configuration.

Finally, some plots proved better than others in terms of quality for the broader study of fuels and fire behavior. In some cases, plots did not burn in the prescribed fire or burned with unusual patterns. In other cases, equipment malfunctioned resulting in poor or missing data. For example, TIR imagery was not obtained for a several plots, and erroneous gain settings were used in others. Therefore, the focus of this thesis is on plots with the highest-quality data end-to-end,

although fuel polygons and attributes were produced for all non-BICO plots in 2018 and 2019. In this thesis, the results for all plots are generally shared in appendices while the high-quality plots become the focus of analysis in the body of the thesis document. In 2018, a subset of the plots in the Brattain burn unit were the focus of analysis. In 2019, all of the plots not within the BICO units were the focus of analysis. A complete set of STANDFIRE inputs was developed for all plots and delivered as shapefiles with attribute tables. Attributes that were not obtained from this research such as surface area to volume ratio, and particle density are defaults from STANDFIRE that can be changed by future users to suit their needs.

## 2.2 Data Collection and Processing

Plots were located within the BICO East, BICO West, Brattain, and Coyote South burn units (Figure. 1). They are 100 x 100 m in size and monumented with rectangular steel plates which



*Figure 2. 2017 painted numbered GCP, 2018 GCP polished steel plate and 2019 GCP*

were visible in the drone imagery. In the first year of study (2017), white 40 x 40 cm plates with large black numbers in the center (Figure. 2) were placed to create a 10 x 10 m square embedded plot within an outer 100 x 100 m square plot. The corners of each plot were marked with one of the white plates, without any specific cardinal orientation.

The centers of these plates were recorded using a cellular phone global positioning system (GPS) unit with a reported accuracy of  $\pm 2$  m in X, Y and Z values (Merry and Bettinger 2019), and occasionally with a Trimble GPS unit (grass north and south). The white paint plates are clearly visible in the RGB-NIR imagery, which allowed them to be used as ground control points (GCP) later in the processing of the imagery.

In the second year of study (2018), to help georeferencing and rectifying imagery later in processing, plots were laid out with 40 x 40 cm polished steel plates (Figure. 3). One inner embedded square plot of 10 x 10 m was nested in the center of the outer square plot of 100x100m. Each corner was marked with one steel plate and the steel plates were oriented magnetic North-South. The Northwest and Southeast corners of the plates were recorded using Emlid RS+ GPS unit acquiring data in real time kinematic mode (RTK), which created a locally accurate measurement of position for each plate based on a locally known base station which then corrects for error to the rover in real time. The use of this RTK GPS system greatly increased the accuracy of the locations in the experiment to about  $\pm 20$  cm in X, Y and Z values (Guo, Ji et al. 2001).

The third year of study (2019) again used 40 x 40 cm polished steel plates with a 3-inch hole drilled in the center (Figure. 3). One center plate was placed within a clear view of the sky, two more plates were placed within  $\sim 50$  m in clear view of the sky from the center plate on either side in an L shaped pattern. The outer plates were then placed on a 100 m diagonal from the



center plates oriented true north. Each plate was then marked on the center hole using an Emlid RS2 dual frequency GPS unit running in RTK mode. Again, in the third year of the study accuracy was increased using the dual frequency GPS units. In this year the reported accuracy was reduced down to  $\pm 25$  cm X, Y and Z values (Guo, Ji et al. 2001, Tripcevich 2017).

When using both the Emlid RS+ and RS2 GPS units the user can set up accuracy thresholds for each type of data point (single, float, fix). If the accuracy of the point was not within the allotted threshold during the collection time, then the point could be manually accepted by the user or recollected to make sure the accuracy needed was achieved when collecting the point. In each of the years the goal was to achieve better accuracy using new technology. Other experimental considerations when placing and choosing the material of the GCP's were considered, such as exploiting the emissivity of the plates to act as thermal GCP's during fire data collects.



*Figure 3. DJI M100 quadcopter*

For each plot, data was collected with the best visible lighting conditions possible to alleviate shadows but also accounting for the limited amount of time allotted to collect the imagery before the plots were burned or pre-burn field days were complete. The type and quality of data collected varied by year (described below), reflecting

improvements in methods and advancements in mission planning software from year to year.

Pre-fire data was collected to produce visible orthomosaics and 3D point clouds to characterize

fuels variability. Data was collected using a DJI Matrice M100 quadcopter with dual 5700mAh batteries (Figure. 3), using three different cameras. The Micasense Rededge 3 (MSRE) multispectral camera (blue, green, red, near infrared, red edge) (2018, 2019), the gimbaled DJI X5 16-megapixel RGB camera (2017), and the gimbaled DJI X3 12-megapixel RGB camera (2018, 2019). The X3 and X5 were mounted on a gimbal to compensate for the aircraft's roll, pitch, and yaw differences in flight. This compensation for the UAS attitude allowed for more control in the sensor's ability to capture NADIR images and allowed for more efficient, effective data collects, allowing sidelap and endlap to be reduced while still achieving the proper amount of endlap and sidelap for processing of forested areas using Agisoft. By reducing the amount of sidelap and endlap the missions were able to be flown in one or two battery cycles. The Micasense was mounted in a fixed 10° forward facing mount, this mount was used to compensate for the forward leaning aircraft during flight, and this was done to better achieve a NADIR photo from the fixed mount. Both cameras collected imagery simultaneously but were offset approximately 20 cm from the focal center of each camera. All photo exposure points were automatically calculated for the endlap and sidelap for each mission within Map Pilot's Pro

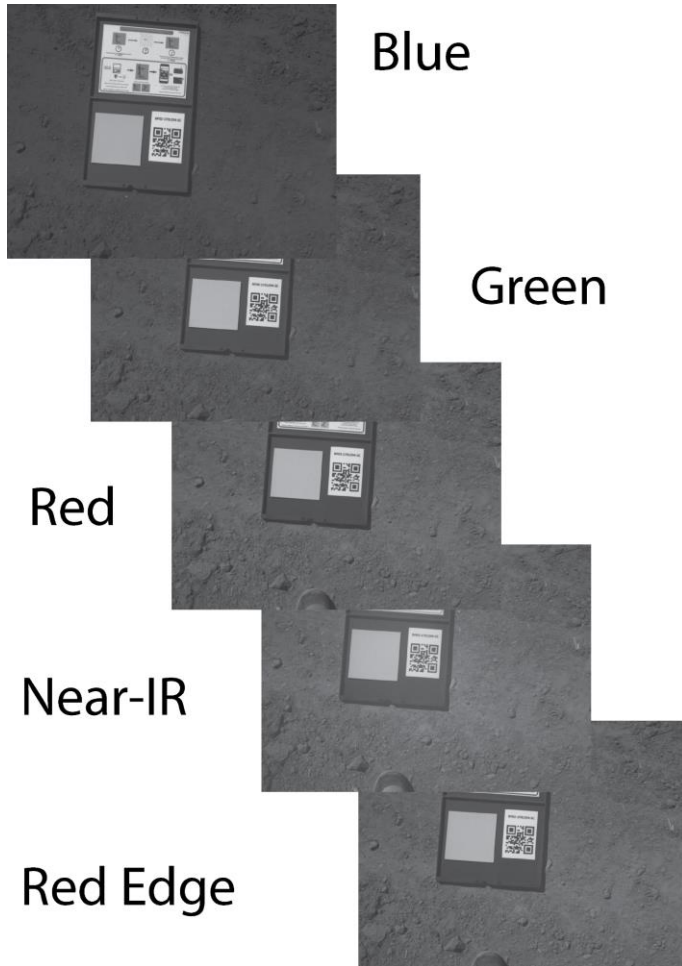


Business Edition (Figure. 4).

To develop flight plans, the outer plot points were imported into Map Pilot's Pro Business Edition (versions 2.5.0-4.1.2) as a KML layer to mark the outer edges of

*Figure 4. Map Pilot's Pro Business Edition flight plan*

the plot from Avenza maps. A square box was created with approximately 2.5-3 hectare for the flight mission using Map Pilots, at 90-100 m above ground level (AGL) flying a cross-grid pattern North-South, then East-West, with 85% endlap and 90% sidelap (Figure. 5). This endlap and sidelap was calculated for the RGB cameras to equate to a 75% sidelap with the micasense camera. This was needed because the MSRE and the X3/X5 have different resolutions. When



imaging forested areas it is recommended that endlap and sidelap be high due to forested areas having very little structure and geometry within each image and this is especially true when imaging closed canopy forest stands (Carrivick, Smith et al. 2016). Map pilots allow the use of terrain following using the Shuttle Radar Topography Mission (SRTM) terrain tiles cached to the Map Pilots application. Using terrain following allowed the UAS to maintain a constant height above the plot area, allowing for a more consistent

*Figure 5. Micasense calibration panels bands 1-5*

Ground Sample Distance (GSD) across the entire acquisition, as well as efficiently keeping the endlap and sidelap to a constant distance. Although having SRTM was not crucial for these data collections as there was very little elevation change from one end of the plot to the other in either direction North-South or East-West, it was used to maintain constant flight elevation. Each

mission was on average 25 minutes per flight for the entire cross-grid, resulting in on average 500 photos with the X3/X5 and 5000 photos with the micasense red edge. The difference in the number of photos collected is due to the micasense capturing Red, Green, Blue, Red edge, and Near-infrared (NIR) bands. Before each flight and before each battery change images of the micasense calibration panel (Figure. 5) were taken in the fullest view of the sun and without any shadows. Together with the calibration panel and the daylight sensor (DLS) the micasense can account for a change in solar angle and cloud conditions by calibrating the photos in metashape after importing them. All images were captured in raw format without editing any aspect of the photo before importing them into the processing software.



*Figure 6. 1m<sup>2</sup> square photoload sample plot*

Field data were collected in all three years (2017, 2018, and 2019) of the study, with significant differences in methods between years due to advancements in technology and evolution of thinking from year to year. The between-year variability in field methods is primarily due to the locations of the field plots (sampling

strategy) and the accuracy of measurement of sampled locations. The information collected on each field plot in each year was essentially the same with a bit of between year variability (only shrub heights taken was in 2018). The variability in methods is a major reason this project has adopted the polygon as the spatial unit of analysis rather than the pixel. Field plots were 1 m<sup>2</sup> areas, as squares (Figure. 6) in 2017-2018 and circles (Figure. 7) in 2019. The following data

were recorded within each field plot using the photoload (Keane, Dickinson et al. 2007) sampling technique: percent cover for grass, bare earth, litter, CWD, 1 hour, 10 hour and 100-hour, grass, and litter fuel load estimates, average fuel heights, and litter depth. In 2017 field plots were randomly distributed by throwing CDs into the plots and referenced using a consumer-grade cellular phone GPS. Field data collected in 2018 plots were distributed near plot monuments to characterize the diversity of fuel types within the plot and referenced by distance and bearing from the monumented plates used to mark the plots using a compass and laser rangefinder. Plot monuments were referenced using an Emlid RS+ RTK GPS as mentioned earlier. The areas sampled were a 1 x 1 m square. In 2018, shrub field measurements were also taken, consisting of width two times (north-south and east-west) and height for 42 sages, bitterbrush, and rabbitbrush. One issue with using the square sample areas is that the spatial orientation needs to be consistent within each photo.

Field data collected in 2019 used Emlid RS2 multi-frequency RTK GPS to collect all sample points. The general locations of sample points were identified ahead of time from a single overhead drone image using visual texture and tone as the basis for identifying fuel type differences. In the field, field samples were distributed



*Figure 7. Hula-Hoop photoload sample plot*

across the range of textures and tones arbitrarily but ensuring an adequate sample size within each strata. Fuels plot boundaries were defined by a circle (hula-hoop, Figure. 7) instead of a square. Within the hula-hoop percent cover for grass, bare earth, litter, and shrub were recorded. One hour, ten hour and hundred-hour fuel estimates, average grass heights, average grass fuel loading, litter depth measurements were also taken. Load measurements used the Photoload technique as in 2018. Using round sample areas with the GPS point avoided the orientation issues associated with square sample areas.

Pre-fire imagery was processed using Agisoft Photoscan and Agisoft Metashape (versions 1.4.0-1.7.2) structure from motion (SfM) software (Figure. 8) using multi-node processing on five computers at one time. The RGB photos were brought into metashape via the import photos tab and a quality assessment was run on each photo. Photos that did not meet the standard quality assessment of 0.80 and above were culled from the processing stream. The number of 0.80 was decided based on assessing all the photos quality assessment and noticing a large gap from 0.80 to 0.60 and looking at where those photos were within the data collect. Most of the photos below the 0.80 threshold were where the UAS was turning into another flight line and motion blur was quite large because of the yaw of the UAS. Because of the location of these photos, they were able to be deleted. It is

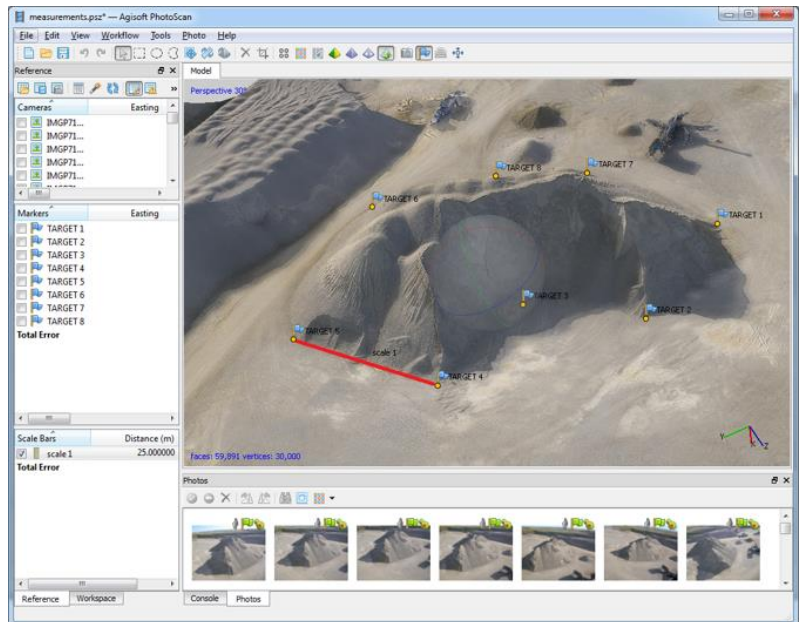


Figure 8. Agisoft Metashape processing

worth pointing out that sometimes a photo that does not meet the quality assessment cannot be thrown out due to its location within the other data collected.

The micasense photos processing stream was slightly different from the RGB camera. They are natively organized in photo sets of five (Red, Green, Blue, Red Edge and NIR). Once selected, metashape prompts the user to bring the cameras in as single cameras or groups of multi-spectral cameras. The multi-spectral option was used and the micasense images were then calibrated based on data from the on-ground reflectance panel and from EXIF data within each photo from the onboard daylight sensor (DLS). Once the multi-spectral micasense images are calibrated the processing stream is the same as the RGB camera except one may have to adjust the brightness depending on how the photos look after calibrating reflectance.

Once photos from both cameras were adjusted, calibrated, and corrected they were each aligned to create a sparse point cloud using the highest accuracy, generic preselection, and reference preselection, key point limit set to 40,000, tie point limit set to 4,000, and adaptive camera mode turned on, these are all default options within metashape. Once the photos were aligned and GCP's in NAD 1983 UTM zone 10N were imported into metashape from a CSV. Aligned camera position thumbnails were turned on to show where each photo exposure point was within the sparse point cloud. While maintaining a NADIR look within the sparse cloud, the model was moved to the four inner GCP's and photos that were near these inner four GCP's were selected, and the imported points used to mark the GCP were placed on the physical GCP shown within the photo. As GCP's are moved in metashape to match GCPs in the images Metashape updates the model and places the other GCP's where it thinks they should be. This is oftentimes very close to where they should be placed but oftentimes the point was manually fine-tuned to home in the accuracy of the GCPs. Once the four inner GCP's are marked in a minimum of three

different images (the more images with GCP's marked in photos, the more accurate the model metashape will be produced). The outer four GCP's were then marked using the same process as the inner four. Photos that contain the GCP's marked by metashape are depicted with blue flags and photos that contain GCP's manually marked by the user are shown with green flags. Once all GCP's are marked, all the photos are deselected, and the sparse model is optimized and updated with the new GCP model. The sparse point cloud is then filtered using three gradual selection criteria, reprojection error, reconstruction uncertainty, and projection accuracy. There is no hard-fast rule for each of these filtering criteria, but a good general rule of thumb is to get rid of ~10% of the points within the sparse point cloud each time (Carrivick, Smith et al. 2016). Once gradual selection is complete the project is saved as a .psx project, then it is reopened, and under project settings the camera, coordinate, and marker reference are all set to NAD 1983 UTM Zone 10N EPSG:26910 and saved as a .psz project.

The next step in the workflow requires the user to invoke a python script that runs a Monte Carlo analysis on the sparse point cloud (James, Robson et al. 2017). This script injects noise into the sparse point cloud 2000 times or how many times the user chooses to. After each iteration of noise, the overall error associated with the GCP's is reduced until the reductions become negligible. We found that 2000 iterations were more than enough as after that the results were not worth adding more. Once the script is complete it saves the project in metashape and exits the script within the program. The new saved project is then resaved as a .psx. The reason for saving between different extensions is because of the way the file structure is built for each project type. One file structure (.psx) allows the user to do parallel processing (multi-node, more than one computer) and the other file structure (.psz) only allows the user to process on a single machine (node). Multi node processing or "parallel processing" as Agisoft calls it can greatly



speed up the processing of projects reducing the amount of time needed to complete a project (Han and Hong 2019). This is a very important consideration as often land managers only have a small window to accomplish ecological objectives or small windows in which they are approved to burn due to many factors such as airshed and weather. Once the Monte Carlo process completed and as much of the error as can be removed has been, it is time to build the dense point cloud. The following settings are used when building the dense cloud: quality set to ultra-high, depth filtering set to moderate, and reuse depth maps and calculate point colors checked. Building depth maps and the dense cloud is the most time-consuming process in the workflow and it can oftentimes take two plus days to finish this process depending on the number of photos and area you have as well as the processing power. After the dense cloud completed it is exported from metashape in LAS format, using the WGS 84 UTM Zone 10N EPSG: 26910 projections. Ground points must now be classified using the classify ground within the batch processing window in metashape. Ground is classified based on all available points within the dense cloud using max angle of 15 degrees, max distance 1m, and cell size 50 m, these are all default ground classification settings in metashape and (Bhandari, Oli et al. 2015, Çelik, Alptekin et al. 2020) were found to produce dependable realistic digital surface models (DSM). After classifying the ground points, the DSM was built using the classified ground points using the following settings: projection type is geographic, projection WGS 84 EPSG:4326 as this was what the original data was produced in. The source data is the dense point cloud, interpolation enabled, point classes: ground. The DSM is then used to build the orthomosaics with the following parameters, projection type is geographic in WGS 84 EPSG:4326, built from the DSM surface, refine seamlines, and enable hole filling both turned on, after the process was complete both orthomosaics and DSM were exported as .tiff files in WGS 84 UTM Zone 10N EPSG:

26910 projection for further processing in ArcGIS and LASTools. After exporting the orthomosaics, DSM, and the 3D point cloud all plots were trimmed to an approximate buffer of 50 m outside of the original 100 m plots. This was done to reduce edge effects and was accomplished using ArcGIS clip raster feature and the LASTools cliplas tool.

### **2.3 Derive Fuel-type Polygons using Photointerpretation**

Fuel polygons were derived by delineating areas of distinct fuel characteristics (e.g., shrubs, grasses, litter, and bare earth) on orthomosaics. The method used for polygon delineation-classification was based on traditional photo interpretation (Lillesand, Kiefer et al. 2008).

Polygons were derived through traditional photointerpretation to mimic the approach that most fire managers will take and could do. The fuel polygons were delineated using traditional photo-interpretation methods of association, tone, texture, color, and hue (Avery 1966). Preliminary analysis of orthomosaics showed that litter fuel is closely associated with the presence of trees as well as the red hue from the dead needle cast spread on the forest floor (Figure. 9). Another major cue was the difference in texture between a grass dominant fuel class and a shrub dominant class, which is evident in the orthomosaics as is the difference in texture between bunch grass and cheatgrass. Color played a key role in creating fuel polygons among the grass classes as well as the cheatgrass had a lighter tan color than the bunch grasses and smoother texture. The difference in color from the shrub fuel class compared to the grass fuel class allowed an easy distinction when deriving those fuel classes (Table. 2).

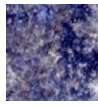




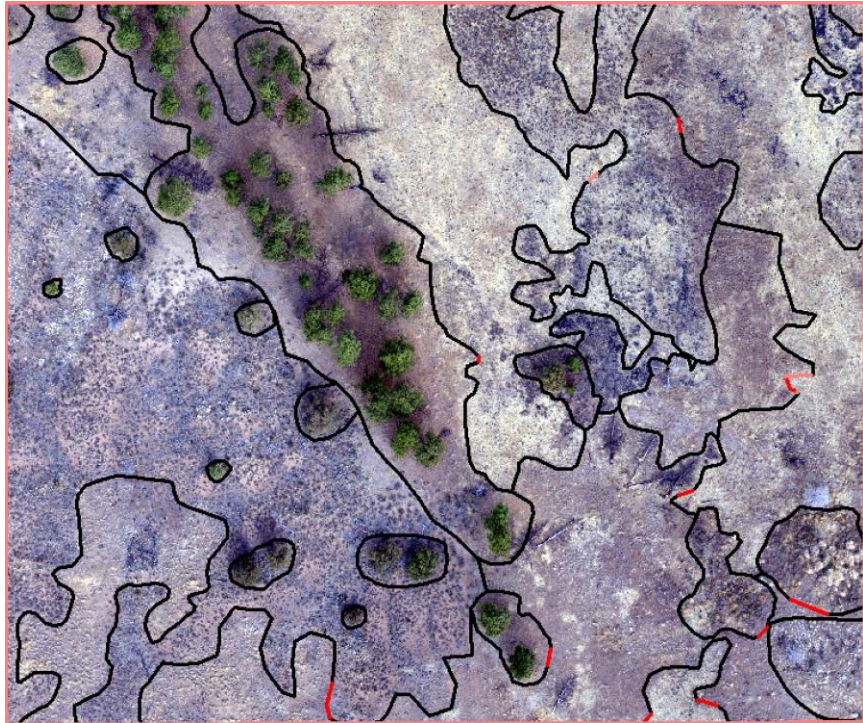
<b>Land Cover</b>	<b>Tone</b>	<b>Texture</b>	<b>Description</b>	<b>Image</b>
Bare	Black/Gray	Rough	Dark black in color with lighter shades of gray. Does not exhibit any spectral difference in NIR.	
Litter	Red/Brown	Smooth	Reddish brown tone that is not found elsewhere in imagery as well as association with the presences of trees.	
Bunch Grass	Golden/White	Rough	White golden patches intermixed among the red bare mineral soil.	
Cheatgrass	Tan/White	Smooth	Continuous cover of tan, brown and white with interspersed black.	
Shrub	Silver/Gray	Rough	Patchy silver-gray objects intermixed among the red bare mineral soil. Some shrubs exhibit spectral difference in NIR.	

Table 2. Photo-interpretation key

The main reason for choosing photo interpretation over spectral and height classification is the fact that land managers will often have access to this type of information readily from UAS imagery, National Agriculture Imagery Program (NAIP), and related sources and may be unable to classify fuels using more automated but more complex image classification techniques such as segmentation and unsupervised/supervised image classification. These maps will provide a point of reference for automated techniques that may be developed in the future.

Using orthomosaics created from UAS RGB imagery with a ground sampling distance (GSD) between three to eight centimeters, four fuel classes (grass, shrub, litter, bare earth) were manually delineated using ArcGIS. The fuel polygons were drawn on the orthomosaics using a Microsoft Surface Pro Four laptop using the stylus pen and the polygon tool on the draw toolbar within ArcGIS. The stylus allowed better control and a much quicker way to manually draw the polygons although it was not necessary and a simple mouse with the polygon tool could also be used. Polygons were originally drawn on the orthomosaics as graphics and they were converted from a graphic to a shapefile and exported into a geodatabase. Due to the fact there were often small gaps and overlapping areas between the polygons that modeling software may have

difficulty differentiating or dealing with, any overlap or gaps in the polygons were corrected using the ArcGIS topology rules to create “pure” polygons that represent a dominant fuel type within that polygon (Figure. 9) Two topology rules were used to identify areas of concern within the polygons. The first rule was



*Figure 9. Brattain H topology rule used to correct polygons*

“must not overlap” and the second rule used was “must not have gaps.” The ArcGIS topology rule does not automatically fix the areas of concern but just searches, finds, and marks the mistakes in red so they can be corrected later. Gaps and overlaps were then corrected by using the editor toolbar and the snap to vertices tools within ArcGIS to get rid of all the overlap and gaps in the shapefiles.

## **2.4 Attribute Fuel Polygons from Field Measurements**

Following derivation of polygons using photointerpretation, each polygon was attributed with fuels data collected in the field, guided by the input requirements of the STANDFIRE translator program. To complete attribution, field plots were extracted by fuel type polygons, summarized, and compared statistically (ANOVA) to fuel attributes from other fuel type polygons. Not all fuel type classes contained a sufficient number of field plots for statistical analysis, so data from

different burn blocks were combined in such cases. In 2019, overhead photos were taken prior to field sampling to aid in sampling field fuel variability within the plots. The idea was to identify tone and texture differences in the plot area quickly in order to ensure that field plots were distributed across the range of variability. This effort normalized the number of samples within each fuel type in 2019, allowing decisions about aggregation of field fuel attributes to be based on statistical differences rather than small sample sizes.

To determine if field plot data from different fuel type polygons could be aggregated, analysis of Variance was run in RStudio to assess differences between fuel classes. If there was a statistically significant difference, a Tukey Post Hoc test was run in RStudio to determine which fuel classes were different. Fuel attributes in fuel types with no significant differences were aggregated. For all the fuel sample and photo-load plots in the polygons, the mean, median, and standard deviation (SD) for percent cover, shrub height, shrub width, litter depth, one-hour fuels, ten-hour fuels, and fuel load ( $\text{Kg/m}^2$ ) and 100-hour fuels were calculated for all fuel classes for entire burn units (aggregated 2018) and for each plot (individual 2019). To check the distributions for normalcy, skewness and kurtosis were calculated for each field measured variable.

Finally, some adjustments were necessary to produce complete attributes for STANDFIRE. STANDFIRE requires estimates of fuel height, cover, loading, and patch size along with bulk density, surface-area-to volume ratio (SAV), and particle density to create LAYERSETS that distribute fuels rationally within polygons. Height and cover for grasses and litter were characterized in the field data in 2018. In 2019 height and cover for grasses, shrubs and litter were characterized in the field data. Loading for grasses and patch size for shrubs as well as bulk density for grasses were also characterized in the field in 2018 and 2019 data but SAV, particle density, patch size for grasses and litter, integer code, and particle density values were not captured in the field data and therefore I used default outputs from STANDFIRE that can quickly be changed within the shapefiles attribute table if it needed to match new world values or values that are actually represent measurements from the burn units being modeled.

Because shrub cover was absent from the field data collections methods, three methods were used to determine shrub percent cover information for STANDFIRE. In the first method,

shrubs cover was estimated ocularly from the photos taken of the field plots during the photoload



*Figure 10. Sample photo-load used for field data*

sampling and summarized by fuel type polygons as described above (Figure. 10). This is effectively the same method used in the field to measure percent cover of grasses and bare earth.

The second method was to create a 15 x 15 m fishnet with points labeled (Figure. 11) using the clipped orthomosaics as the bounding box to perform a dot/grid sample. Each fuel class was used to clip the fishnet and if one of the labeled points fell on a shrub within the orthomosaics it was tallied as a yes or if it did not fall on a shrub a no. Once all points were identified

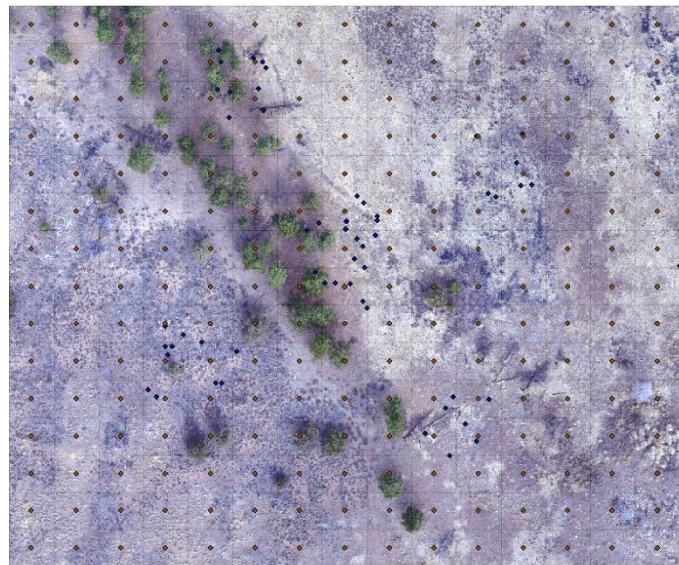


*Figure 11. Example of fishnet plot used to estimate shrub cover*

the total number of points that fell on shrubs were divided by the total number of points within that fuel class polygon to estimate shrub cover using the orthomosaics. At the end, the total number of points in the entire Brattain unit that fell on shrubs was also divided by the total points to estimate a total percent cover shrub for the entire burn unit.

The third method used to determine shrub cover exploited the 3D point cloud elevation data converted to a 2D height raster. The logic was that shrubs had measurable dimensions (height, width) above ground, and were therefore quantifiable by identifying positive elevation anomalies in the surface fuel bed area of the point clouds. In ArcGIS, the point clouds were converted from a 3D .las file into a 2D .tiff elevation raster using the las to raster function within ArcGIS. When using the las to raster function the following settings were applied to all the point clouds: elevation value field, binning Cell Assignment Methods set to nearest and void fill method to none, using floats, sampling type is cellsize and the size of cells is set to what each plot GSD



was, and the z factor is left at 1 meaning no change in actual values. After converting the 3D point clouds into 2D images the tree canopies were masked out of the image using ArcGIS. Using the raster calculator, all points above 2 m were selected. Using the 2 m and above raster as a spatial mask and adding a 2m buffer, tree canopy points and the noisy height data around tree driplines was removed by clipping from the raster using the raster clip function. The remaining raster was considered the canopy height model (CHM) of the fuel bed and included all fuel bed points from the ground to 2 m height. The raster calculator was then used to create a conditional statement ( $\text{Con}(\text{raster} \geq .25)$ , raster) to clip all points 0.25 m and above to create a new raster of shrub heights as determined by the modeled vs field measured shrub measurements. Once the shrub heights were calculated the raster had to be smoothed using a 3 x 3 cm focal maximum filter to remove the anomalies and noise created from the raster calculator (Figure. 12). After smoothing the raster was reclassified using a conditional statement ( $\text{Con}(\text{raster} \geq .25)$ , 1) in the raster calculator to ones and zeros with one assigned to shrub and zero to no shrub. Finally, shrub

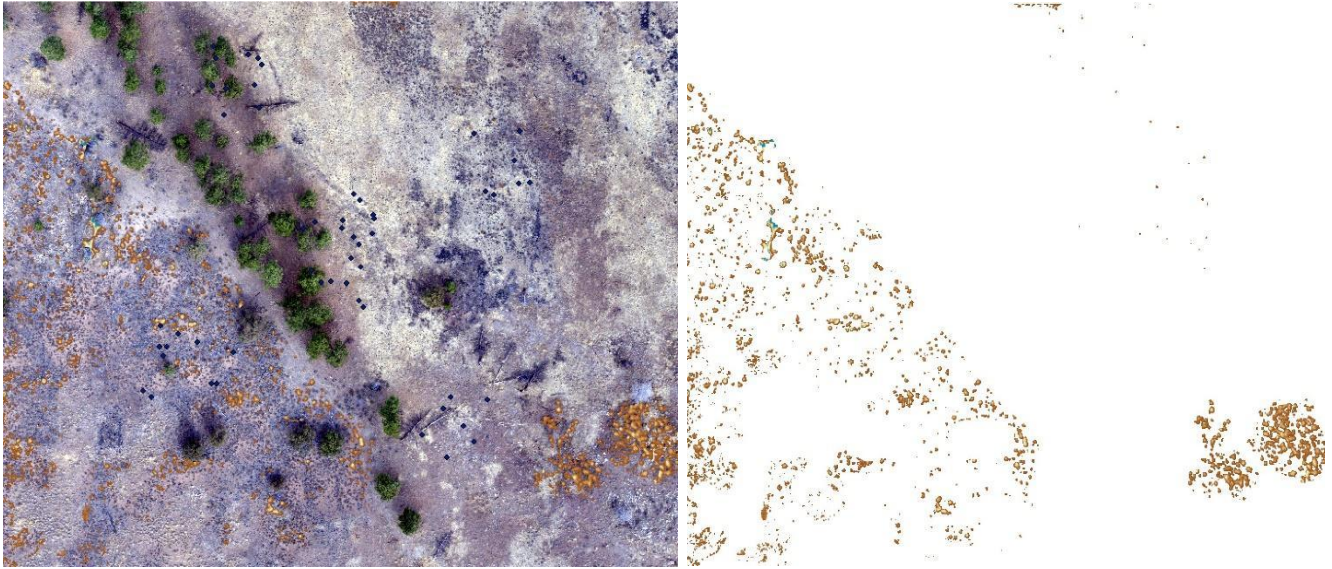


*Figure 12. Rasterized shrub heights Brattain H*

area was calculated using the zonal geometry as table function. The shrub area was then divided by the total area of each fuel class polygon to get an estimation of shrub cover.

## **2.5 Quantify and Compare Shrub Heights and Widths**

An advantage of data from 3D point clouds is their ability to characterize structure, height, and dimensions. These measurements can potentially be used directly to get at metrics such as fuel bed height or can be used to inform classifications of fuel characteristics. For example, Moran (2019) used point-cloud based height measurements to classify fuels at Lubrecht Experimental Forest, MT from imagery collected just a few meters (5-10 m) above the fuel bed. A preliminary analysis of UAS point clouds from Sycan Marsh obtained from imagery collected at 90-100 m AGL suggests that height may not be well characterized in the surface fuel bed. A 2-part approach was used to understand how fuel bed heights and widths are characterized in the 3D point cloud. The first is to compare height and width measurements of shrubs in the point cloud to field measurements of shrubs collected at Sycan Marsh in 2018. Because the field locations of the shrubs are not precise, a search radius of 2 meters around each shrub point in the rasterized

point clouds was used to identify matching shrubs if a shrub was outside of the search radius it was discarded. When more than one shrub appeared in the search radius, their dimensions were averaged. If the object nearest the point was doubtful to be a shrub due to its shape or dimensions, an NIR orthomosaic was consulted to confirm that it was a shrub and not a rock, which look similar in the orthomosaics.

In addition to the shrub-to-shrub comparison described above, ten random points were generated using the ArcGIS random point generator feature (Figure. 13) and from these ten points, the closest shrub visible in the orthomosaic was measured in the CHM. The highest pixel value in

the shrub nearest to each random point represented shrub height. Widths were measured twice and averaged, once north-south and the second east-west.

The data from these shrubs were summarized in box-whisker plots and compared to the similarly summarized field measured shrubs. Measuring in this

manner-maintained consistency across plots, and using the random points helped

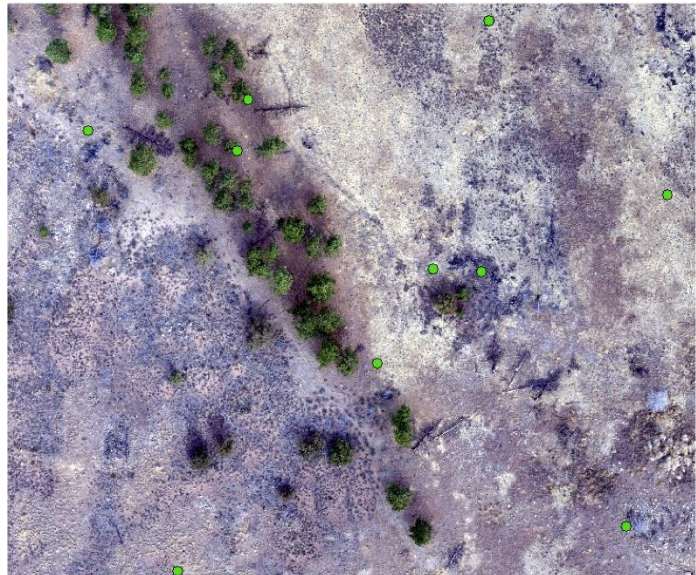


*Figure 13. Random points for shrub measurements*

determine if field measurements of shrub dimensions are similar to point cloud measurements.

## **2.6 Derive a ground surface for generation of the CHM**

In order to develop the canopy height model (CHM) used in the shrub dimension assessment described previously, it was necessary to create and smooth a bare earth model from the point clouds. Using the DSM output from Metashape a bare earth model was created using ground

classified points in a two-step approach; in the first step, the dense point cloud was divided into cells of a specific size. Within each cell, the lowest point was detected. Once the lowest points were detected triangulation of these points gave the first rough calculation of the terrain model. Additionally, at this first step, Metashape filters out some noise points to be handled as low points class. In the second step, new points are added to the ground class, providing that it meets two conditions. First, the point lies within a certain distance from the terrain model and second, the angle between the terrain model and the line to connect this new point with a point from a ground class is less than a certain angle. The second step is repeated multiple times while there still are points to be checked. The three main factors that influence a good ground point classification are the maximum angle in degrees, maximum distance in meters and the size of cells in meters. Due to some of the DSM's having abnormalities related to noise from tree boles, coarse woody debris (CWD) or other above ground anomalies that the ground classification was unable to get rid of, three focal statistics were used to smooth the DSM. The first was a Min filter with a 4 x 4 cm moving window, the second was a Max filter with a 3.75 x 3.75 cm moving window and the final focal stat was a mean (Figure. 14). These statistical sizes were based on multiple outputs within ArcGIS to determine what was the best size of moving window to use.

The approach assumed that the lowest point in the initial Min filter was ground, the following

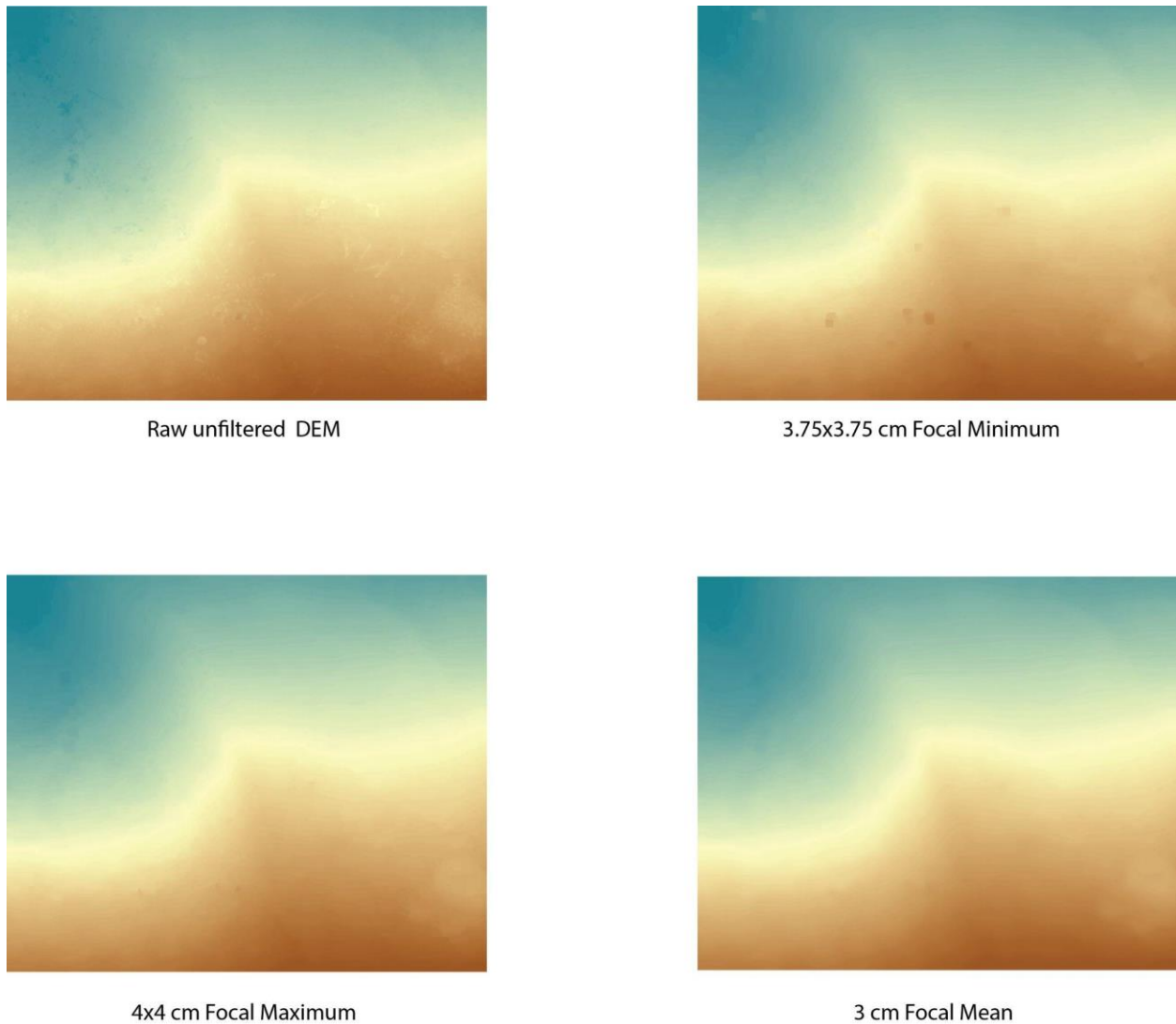


*Figure 14. Smoothing the DSM output from Metashape*

max filter intended to remove erroneous negative noise below ground, and the mean filter then averaged the remaining ‘ground’ point heights.

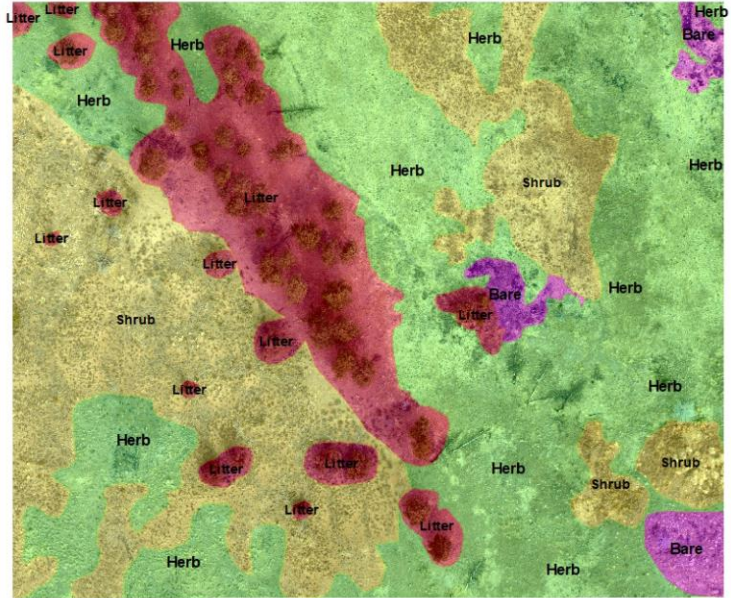
After creating the bare earth model and differencing the point cloud from it (e.g., generation of the canopy height model), the point clouds were converted from 3D las files into a 2D tiff elevation rasters using the las to raster function within ArcGIS. When using the las to raster

function the following settings were applied to all the point clouds: elevation value field, binning Cell Assignment Methods set to nearest and void fill method to none, using floats, sampling type is cellsize and the size of cells is set to what each plot GSD was, and the z factor is left at 1 meaning no change in actual values. 3D point clouds converted to rasters of height. After converting the 3D point clouds into 2D images the tree canopies were masked out of the image using ArcGIS. Using the raster calculator all points above 2m were selected. Using the 2 m and above raster as a mask it was then converted to a polygon in ArcGIS with a 2 m buffer. This created a tree canopy mask that masked out all points that were tree bowls or tree canopies. This new raster was considered the final canopy height model (CHM) and included all fuel bed points from the ground to 2 m height.

## 3. Results

### 3.1 Derive Fuel-type Polygons using Photointerpretation

Fuel polygons were delineated using common photo interpretation methods (Paine and Kiser 2012) and represented by polygons on the



orthomosaics (Figure. 15). Each fuel

*Figure 15. Brattain H delineated fuel polygons*

class polygon is represented on ArcGIS maps as a different color polygon. The following colors on the map represent these fuels, green is grass class (herbaceous), red is litter class, yellow is shrub class, and purple is bare earth (Figure. 16). Each fuel class is not a homogenous class but a representation of the dominant fuel within that area based on the above photo interpretation methods. The total area interpreted for both 2019 and 2018 is 397342 m<sup>2</sup>. For 2018 the total area interpreted is 231323 m<sup>2</sup>. Within 2018 plots, grass fuel classes accounted for 51% (119761 m<sup>2</sup>) of the area, shrubs accounted for 14% (33793 m<sup>2</sup>) of the area and litter accounted for 33% (77768 m<sup>2</sup>) of the area. On a plot-to-plot basis this qualitatively matched what was observed visually while collecting the imagery and installing the GCP's. In 2019 the total area interpreted was 166019 m<sup>2</sup>. Out of the total area in 2019 interpreted 84.1% (139679 m<sup>2</sup>) was considered grass fuel class, shrub fuel class accounted for 4.4% (7271 m<sup>2</sup>) of the total area and litter fuel

class accounted for 4.4% (7354 m<sup>2</sup>). In both 2018 and 2019 this percentage breakdown of fuel classes was comparable to what was observed in the field while installing the plots and collecting the imagery. Many of the plots (SG\_1, SG\_2, grass\_1A and grass\_1C) in 2019 consisted primarily of grass fuels and is the reason why 84% of fuels were interpreted as grass fuel types.

### **3.2 Attribute Fuel Polygons from Field Measurements**

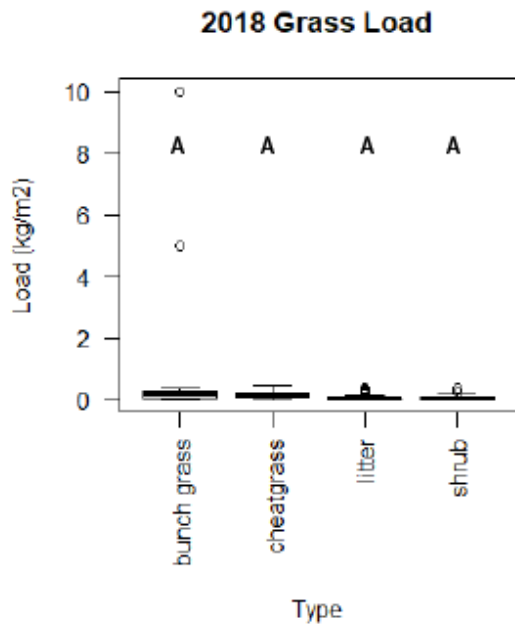
The field data from 2018 Brattain Unit are summarized by plot and fuel type in Table 2. The n/a values represent that the respective fuel class was not present within the plot. Of the 1071 field fuel samples taken in 2018, 306 samples fell within the Brattain unit. Of these, 197 samples were from plots B, C, F and H, higher quality plots that are the focus of this thesis. Of the 197 samples 18 were from the shrub fuel type, 60 from the cheatgrass, 39 from the bunch grass, and 80 were from the litter type. Additionally, some plots had none to a few samples per fuel type. For example, Brattain C had 0 shrub, 1 litter, 0 bunch grass and 1 cheatgrass samples within its boundaries (Table. 2). Given the inconsistent number of field samples among plots and fuel type polygons, it was necessary to aggregate all field data from Brattain into the four fuel type categories, and thus the fuel attributes for each fuel type polygon in any particular plot are the same as in other plots. An analysis of similarities and differences in fuel attributes between fuel types (Box and Whisker plus ANOVA) is shown in boxplots 1-6. It is worth pointing out that every fuel type polygon contains quantities of the other fuels. For example, the shrub type also has grass and litter in it, while the grass type contains some shrub and litter. One might expect that a grass type polygon should have more grass in it than other fuel type polygons given its status as grass, and this is often but not always the case. Boxplots 1-3 suggest that all fuel types have similar grass loads, but grass cover and height are greater in grass-dominant polygons. Additionally, cheatgrass is shorter and has higher cover than bunch grass and this is a common



characteristic of cheatgrass variety of grasses compared with bunch grasses whereas bunch grasses only cover a smaller area while cheatgrasses blanket the entire area. With respect to the litter fuel type (Boxplot 4-5), litter depth and cover are higher than in any other fuel type polygon. The shrub fuel type (Boxplot 6) is confounding because there is no difference in shrub cover across all fuel types, despite shrub type polygons clearly having more shrub cover based on field inspection. This discrepancy is analyzed and evaluated further in section 3.4 below.

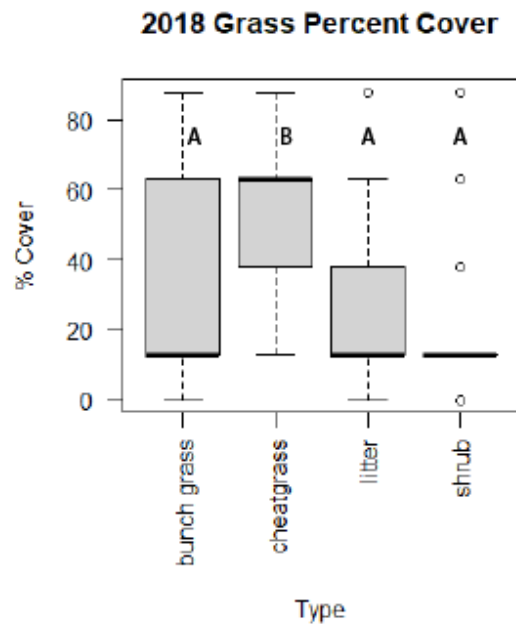
Plot	Fuel Class	N	Percent Cover	SD	Median	Min	Max	Range	Skewness	Kurtosis	SE
Brat H	Cheat Grass	25	49	27.08	38	13	88	75	0.24	-1.32	5.42
Brat H	Bunch Grass	0	n/a	n/a	n/a	n/a	n/a	n/a	n/a	n/a	n/a
Brat H	Litter	15	53	33.81	63	13	88	75	-0.12	-1.88	8.73
Brat H	Shrub	18	3.06	9.26	0	0	35	35	2.59	5.51	2.18
Brat G	Cheat Grass	0	n/a	n/a	n/a	n/a	n/a	n/a	n/a	n/a	n/a
Brat G	Bunch Grass	9	15.78	8.33	13	13	38	25	2.07	2.63	2.78
Brat G	Litter	26	53.38	33.22	50.5	13	88	75	-0.09	-1.56	6.52
Brat G	Shrub	10	0.5	1.58	0	0	5	5	2.28	3.57	0.5
Brat F	Cheat Grass	29	56.1	26.64	63	13	88	75	-0.49	-1.06	4.95
Brat F	Bunch Grass	39	39.9	29.36	38	0	88	88	0.36	-1.36	4.7
Brat F	Litter	6	2.17	5.31	0	0	13	13	1.36	-0.08	2.17
Brat F	Shrub	0	n/a	n/a	n/a	n/a	n/a	n/a	n/a	n/a	n/a
Brat E	Cheat Grass	0	n/a	n/a	n/a	n/a	n/a	n/a	n/a	n/a	n/a
Brat E	Bunch Grass	0	n/a	n/a	n/a	n/a	n/a	n/a	n/a	n/a	n/a
Brat E	Litter	9	51.89	33.33	63	13	88	75	-0.11	-1.92	11.11
Brat E	Shrub	6	0.83	2.04	0	0	5	5	1.36	-0.08	0.83
Brat D	Cheat Grass	0	n/a	n/a	n/a	n/a	n/a	n/a	n/a	n/a	n/a
Brat D	Bunch Grass	0	n/a	n/a	n/a	n/a	n/a	n/a	n/a	n/a	n/a
Brat D	Litter	0	n/a	n/a	n/a	n/a	n/a	n/a	n/a	n/a	n/a
Brat D	Shrub	1	0	n/a	n/a	n/a	n/a	n/a	n/a	n/a	n/a
Brat C	Cheat Grass	1	13	n/a	n/a	n/a	n/a	n/a	n/a	n/a	n/a
Brat C	Bunch Grass	0	n/a	n/a	n/a	n/a	n/a	n/a	n/a	n/a	n/a
Brat C	Litter	1	38	n/a	n/a	n/a	n/a	n/a	n/a	n/a	n/a
Brat C	Shrub	0	n/a	n/a	n/a	n/a	n/a	n/a	n/a	n/a	n/a
Brat B	Cheat Grass	5	44.25	37.5	38	13	88	75	0.14	-2.28	18.75
Brat B	Bunch Grass	0	n/a	n/a	n/a	n/a	n/a	n/a	n/a	n/a	n/a
Brat B	Litter	59	42.24	32.55	38	13	88	75	0.43	-1.6	4.24
Brat B	Shrub	0	n/a	n/a	n/a	n/a	n/a	n/a	n/a	n/a	n/a
Brat A	Cheat Grass	0	n/a	n/a	n/a	n/a	n/a	n/a	n/a	n/a	n/a
Brat A	Bunch Grass	2	25.5	17.68	25.5	13	38	25	0	-2.75	25
Brat A	Litter	37	37.32	28.56	38	13	88	75	0.7	-1.05	4.69
Brat A	Shrub	8	3.75	45.26	2.5	0	90	90	0.42	-2.02	16

Table 3. 2018 Fuel samples summary.



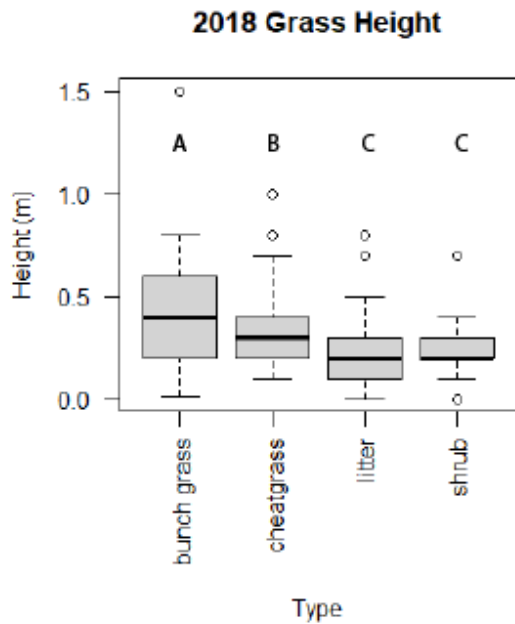
Boxplot 2. 2018 grass load by fuel type

Differing letters above boxes denote statistically significant differences ( $p < 0.01$ ).



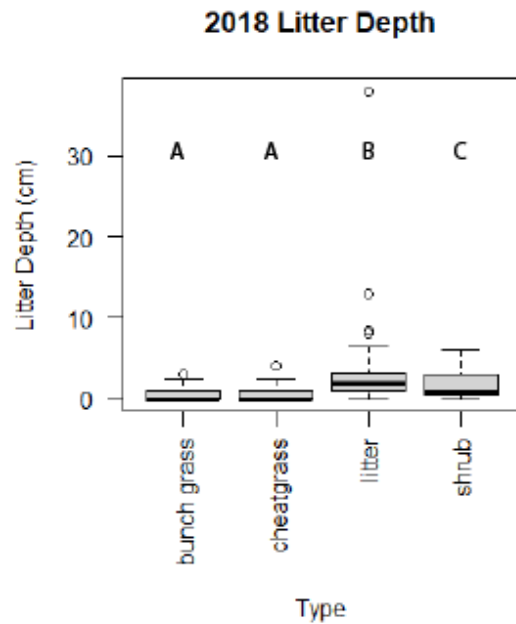
Boxplot 1. 2018 grass cover by fuel type

Differing letters above boxes denote statistically significant differences ( $p < 0.01$ ).



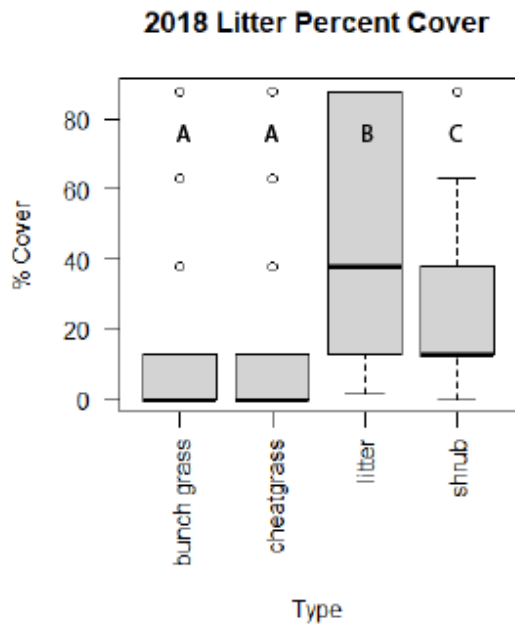
Boxplot 4. 2018 grass height by fuel type

Differing letters above boxes denote statistically significant differences ( $p < 0.01$ ).



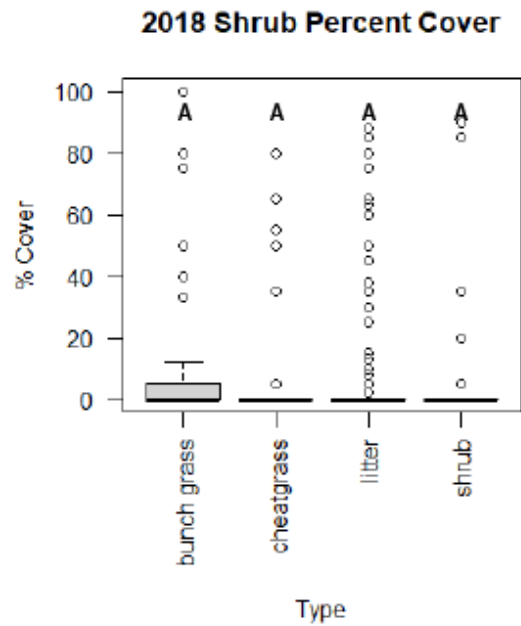
Boxplot 3. 2018 litter depth by fuel type

Differing letters above boxes denote statistically significant differences ( $p < 0.01$ ).



Boxplot 5. 2018 litter cover by fuel type

Differing letters above boxes denote statistically significant differences ( $p < 0.01$ ).



Boxplot 6. 2018 shrub cover by fuel type

Differing letters above boxes denote statistically significant differences ( $p < 0.01$ ).

In 2019, the overhead images (Figure. 17) helped the field sampling of fuels by ensuring that fuel type polygons had a sufficient number of samples. This allowed fuel attributes of each 100 x 100 m plot to be compared with other plots and either combined or kept

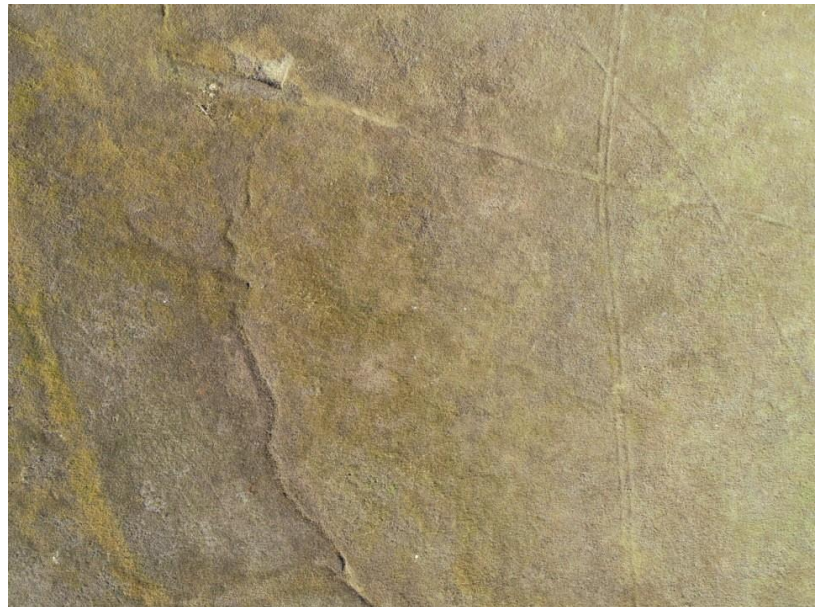


Figure 16. Overhead image to aid sampling

separate plot due to their differences. There was a more consistent number of samples within each fuel type when using the overhead image sampling assisted method (Table. 3). Thus, the n/a in Table 3 represents fuel classes that were not present within a plot rather than a lack of field samples.

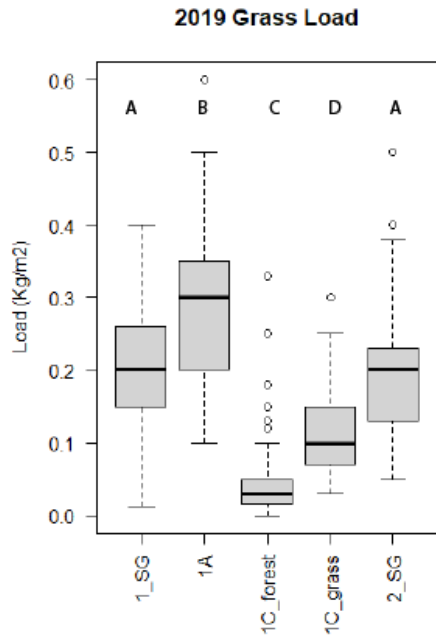
Plot	Fuel Class	N	Percent Cover	SD	Median	Min	Max	Range	Skewness	Kurtosis	SE
Forest_1C	Shrub	21	36.67	35.27	13	0	88	88	0.29	-1.69	7.7
Forest_1C	Bunch Grass	22	44.82	26.93	38	0	88	88	0.05	-1.23	5.74
Forest_1C	Litter	51	74.76	22.56	88	13	88	75	-1.52	1.09	3.16
Grass_1A	Shrub	0	n/a	n/a	n/a	n/a	n/a	n/a	n/a	n/a	n/a
Grass_1A	Bunch Grass	38	84.71	10.35	88	38	88	50	-3.12	9.45	1.68
Grass_1A	Litter	0	n/a	n/a	n/a	n/a	n/a	n/a	n/a	n/a	n/a
Grass_1C	Shrub	0	0	0	0	0	0	0	0	0	0
Grass_1C	Bunch Grass	50	70.5	20.98	75.5	13	75	62	-1	0.2	2.97
Grass_1C	Litter	0	n/a	n/a	n/a	n/a	n/a	n/a	n/a	n/a	n/a
1_SG	Shrub	0	n/a	n/a	n/a	n/a	n/a	n/a	n/a	n/a	n/a
1_SG	Grass	45	81.89	12.1	88	38	88	50	-1.72	2.08	1.8
1_SG	Litter	0	n/a	n/a	n/a	n/a	n/a	n/a	n/a	n/a	n/a
2_SG	Shrub	0	n/a	n/a	n/a	n/a	n/a	n/a	n/a	n/a	n/a
2_SG	Grass	39	84.15	9.14	88	63	88	25	-1.85	1.44	1.46
2_SG	Litter	0	n/a	n/a	n/a	n/a	n/a	n/a	n/a	n/a	n/a

Table 4. 2019 fuel sample summary

In 2019, there were 510 fuel samples taken, 100 in forest\_1C, 38 in grass\_1A, 50 in grass\_1C, 38 in 2\_SG, 45 in 1\_SG, 74 in forest\_1B, and 39 in BICO\_9E\_south, 89 in BICO\_9E\_middle and 43 in BICO\_9E\_north. Out of the 510 samples in the 2019 unit, 216 were from the non-BICO plots and these are the plots used in this analysis (e.g., 1C\_forest, grass\_1A, 1C\_grass, 1\_SG and 2\_SG (Table. 3). Most of the latter plots were in pure grass fuel types (e.g., 1\_SG, 2\_SG, 1A, 1C\_grass). Plot 1C\_grass was distinct as an upland native bunchgrass community while the other grass dominated plots were characterized mainly by rhizomatous marsh/agricultural grass. The only plots that had any fuel type other than grass were 1C\_forest (grass, shrub, litter) and 1C\_grass (grass and shrub). Due to no field fuel samples being taken in a tiny sliver of shrub fuel type in 1C\_grass, this sliver was attributed with shrub data collected in the adjacent plot 1C\_forest. Boxplots 7-13 show field fuel distributions and differences (Box and Whisker plus ANOVA), for each of the 100 x 100 m plots. 1\_SG and 2\_SG which are separated by a mow-line in the field and appear identical, are no different in any attributes and thus, their field measurements were combined to produce STANDFIRE attributes. The rest of the plots were kept separate because of observed differences in one attribute or another. For example, the grasses in 1C\_forest and 1C\_grass are mainly bunch grass. 1C\_forest also has a mix of forest litter fuels plus several shrub type polygons. Grass height is the same in both plots, but load, bulk density, and cover are significantly higher in 1C\_grass. Similarly, Plot 1A which is also exclusively agricultural grass and resembles 1\_SG and 2\_SG in appearance, has a significantly higher fuel load and taller fuel bed. In the end, apart from 1\_SG and 2\_SG grass load was consistently

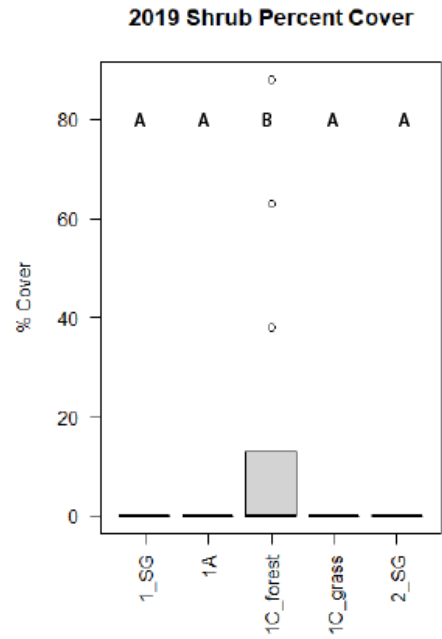
different from plot to plot (Boxplot. 7). Shrub percent cover was similar across the plots within the unit except for 1C\_forest (Boxplot. 8) which is the only plot that had much shrub cover. One hour, ten hour, and hundred-hour fuel loadings (Boxplot. 9-11) had a negligible difference across plots, while litter depth was varied (Boxplot. 12). Other than 1C\_forest there was little litter fuel class within the 2019 units as much of them were grass. Although there were a few fuel characteristics that were similar among the 2019 plots, there were not enough similarities to aggregate them into one unit like what was done in 2018, plus the modified sampling technique of 2019 allowed the area to be sampled on a per plot basis without the need for aggregation as occurred in 2018.

As described previously, the overhead images taken to help aid sampling increased the number of samples taken within all fuels present in the 2019 plots. Because these images showed textural differences in grasses in 1\_SG, 2\_SG and grass\_1A, each had its own fuel classes. For the sake of ease, these two different grass fuel classes were called flat grass and stream grass based on their appearance and the proximity of the latter class to subtle topographic drainages. Further assessment of the grasses and fuel samples from each showed that they were in fact the same grass class and just visually different but with no differences in grass attributes such as cover (Boxplot. 13), grass load (Boxplot. 14) or grass height (Boxplot. 15). Due to these findings, all the grass field data were combined in 1\_SG and 2SG and the flat and stream grass in 1A was also aggregated within that plot. These plots then, are characterized by a maximally homogenous fuel bed. Otherwise, the fuel type polygons are attributed with data only from the photo-delineated fuel type polygons of each individual plot.



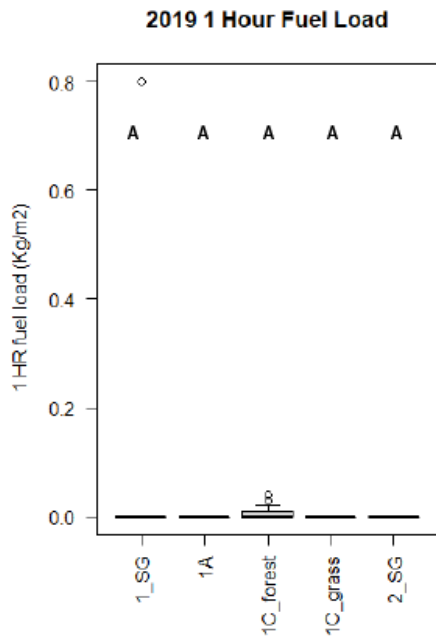
Boxplot 8. 2019 grass load vs. plots

Differing letters above boxes denote statistically significant differences ( $p < 0.01$ ).



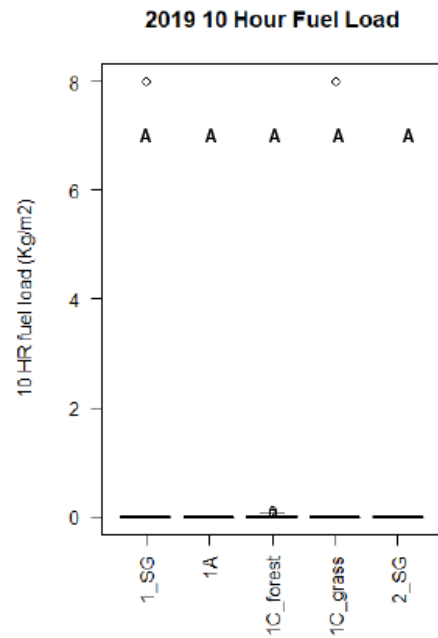
Boxplot 7. 2019 shrub cover vs. plot

Differing letters above boxes denote statistically significant differences ( $p < 0.01$ ).



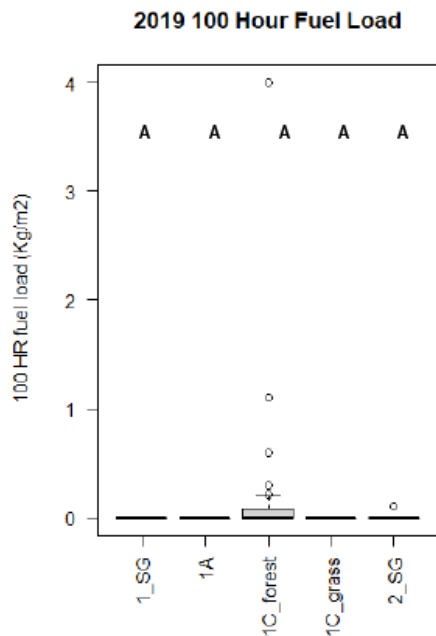
Boxplot 12. 2019 One-hour fuel vs. plot

Differing letters above boxes denote statistically significant differences ( $p < 0.01$ ).



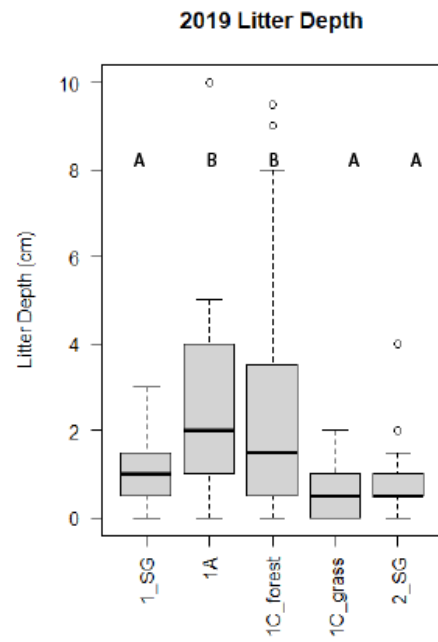
Boxplot 11. 2019 Ten-hour fuel vs. plot

Differing letters above boxes denote statistically significant differences ( $p < 0.01$ ).



Boxplot 10. 2019-hundred-hour fuel vs. plots

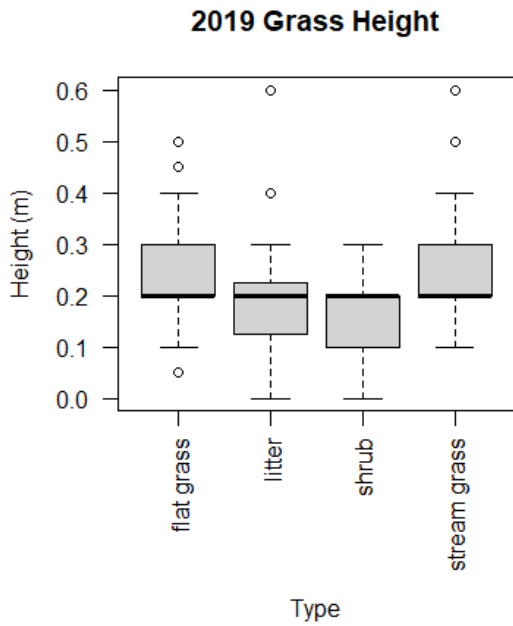
Differing letters above boxes denote statistically significant differences ( $p < 0.01$ ).



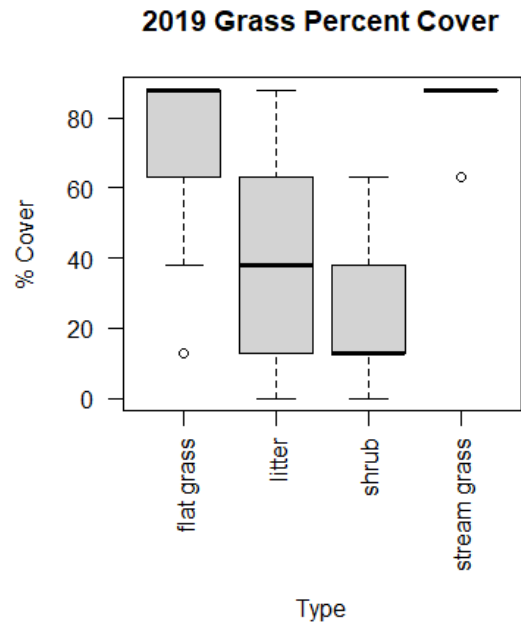
Boxplot 9. 2019 litter depth vs. plots

Differing letters above boxes denote statistically significant differences ( $p < 0.01$ ).

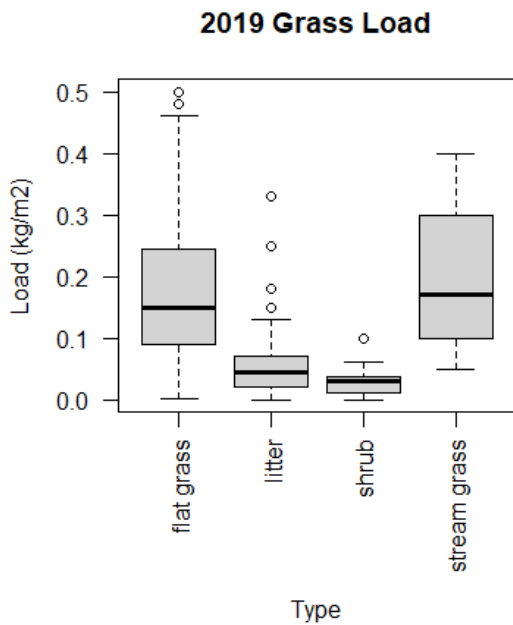




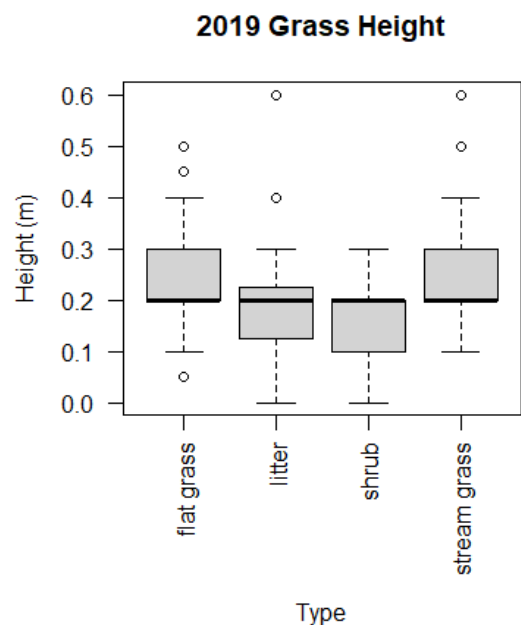
Boxplot 14. 2019 grass height vs fuel type



Boxplot 13. 2019 grass cover vs. fuel type



Boxplot 15. 2019 grass load vs. fuel type



Boxplot 16. 2019 grass height vs. fuel type

### 3.3 Quantify and Compare Shrub Heights and Widths

After identifying shrubs within a designated 2m search radius of field measured shrubs in the point clouds as well as identifying the nearest shrub to the ten randomly generated modeled shrub points (Figure. 21), the dimensions of each shrub were measured manually within the CHM. The data revealed that shrub height was under-estimated (Boxplot. 17) in the CHM shrubs compared to the field

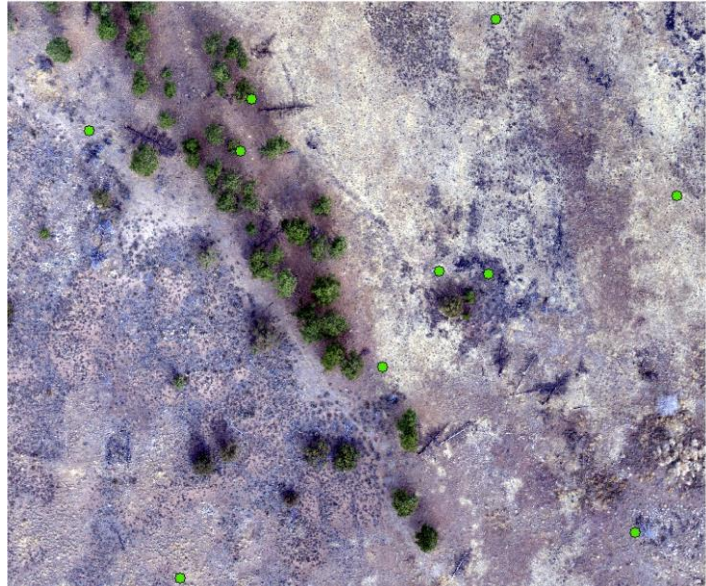
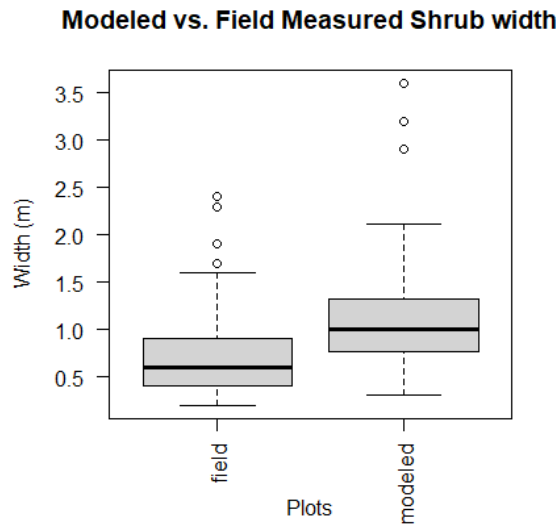
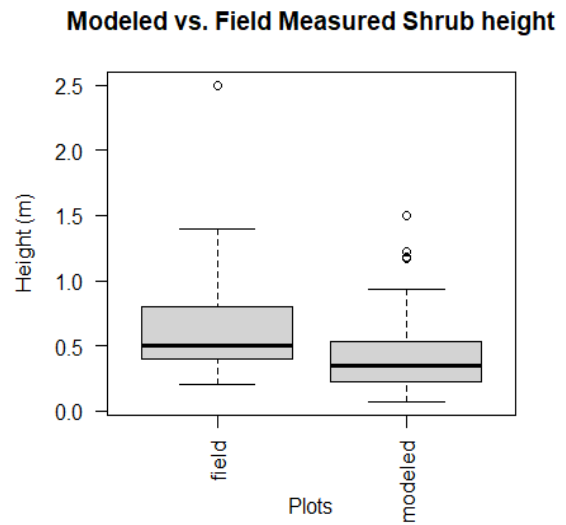


*Figure 17. Ten random points for shrub measurements*

measured shrubs in both the search radii (shrubs that might correspond with field measured shrubs) and at random points (unbiased sample of shrubs). CHM shrub height was about 0.5 times shorter than field measured height. Shrub widths were the exact opposite, where field shrubs were less-wide (Boxplot. 16) than shrubs measured in the CHM. Modeled shrub width was about 1.5 times wider than the field.



*Boxplot 18. Modeled vs. field measured shrub widths*



*Boxplot 17. Modeled vs. field measured shrub heights*

### 3.4 Assess Shrub Cover Derived from UAS Point Clouds

Shrub cover was initially derived from estimates obtained from downward looking photos of fuel plots taken in the field for the Brattain H 100 x 100 m plot. Brattain H was the focus of this investigation because it contained a diversity of fuel types including large expanses of shrublands, and its end-to-end data quality was high. This method produced an overall shrub cover for Brattain H of 11.2% across all fuel types. The dot/grid method across the same landscape produced a shrub cover estimate of 12.5%, and the CHM-derived estimate from the UAS imagery gave a shrub cover of 6.3%. Within fuel polygons that were shrub-dominant (shrub type polygons), the ocular estimate from field photos was 2% (Figure 19), dot-grid was 57% (Table 4), and CHM-derived estimate was 18% (Table 5). These large discrepancies are likely the result of bias in the field sampling for the ocular estimate, and insensitivity to short-statured shrubs in the CHM-derived approach. The old-fashioned dot-grid on a high-resolution

orthoimage produced the best match to field-observed shrub cover, likely due to its unbiased sampling combined with the power of photointerpretation to identify shrubs.

<b>Fishnet Shrub Percent Cover</b>				
<b>Plot</b>	<b>Fuel Class</b>	<b>Present</b>	<b>Total</b>	<b>% Cover Shrub</b>
<b>Brat B</b>	<b>Shrub</b>	<b>1</b>	<b>1</b>	<b>100.00</b>
Brat B	Cheatgrass	3	35	8.57
Brat B	Bunch Grass	N/A	N/A	N/A
Brat B	Litter	15	176	8.52
<b>Brat C</b>	<b>Shrub</b>	<b>33</b>	<b>81</b>	<b>40.74</b>
Brat C	Cheatgrass	6	22	27.27
Brat C	Bunch Grass	N/A	N/A	N/A
Brat C	Litter	9	122	7.38
<b>Brat F</b>	<b>Shrub</b>	<b>3</b>	<b>6</b>	<b>50.00</b>
Brat F	Cheatgrass	2	96	2.08
Brat F	Bunch Grass	5	100	5.00
Brat F	Litter	0	23	0.00
<b>Brat H</b>	<b>Shrub</b>	<b>29</b>	<b>77</b>	<b>37.66</b>
Brat H	Cheatgrass	3	103	2.91
Brat H	Bunch Grass	N/A	N/A	N/A
Brat H	Litter	1	39	2.56
	<b>Total Unit Shrub Cover</b>	<b>110</b>	<b>881</b>	<b>12.49</b>
	<b>Avg. Cover Shrub Polygons</b>			<b>57.10</b>

*Table 5. Fishnet derived shrub cover*

<b>CHM Shrub Percent Cover</b>				
<b>Plot</b>	<b>Fuel Class</b>	<b>Polygon Area</b>	<b>Shrub Area</b>	<b>% Cover Shrubs</b>
Brat B	Shrub	106.20	24.11	22.70
Brat B	Cheatgrass	6715.14	267.06	3.98
Brat B	Bunch Grass	N/A	N/A	N/A
Brat B	Litter	28043.41	967.09	3.45
Brat C	Shrub	14482.85	1152.45	7.96
Brat C	Litter	23500.31	844.38	3.59
Brat C	Cheatgrass	3862.06	246.12	6.37
Brat C	Bunch Grass	N/A	N/A	N/A
Brat F	Shrub	1802.20	627.16	34.80
Brat F	Cheatgrass	25129.88	1452.16	5.78
Brat F	Bunch Grass	26242.15	3549.06	13.52
Brat F	Litter	6159.62	733.39	11.91
Brat H	Shrub	17402.64	1138.54	6.54
Brat H	Cheatgrass	24173.36	638.79	2.64
Brat H	Bunch Grass	N/A	N/A	N/A
Brat H	Litter	8720.59	179.18	2.05
	<b>Total Shrub Cover</b>	186340.41	11819.49	6.34
	<b>Average Shrub Cover Shrub Polygons</b>			18.00

*Table 6. CHM derived shrub cover.*

# 4. Discussion

## **4.1 Objective 1. Derive Fuel-type Polygons using Photointerpretation**

Deriving fuel polygons using photo interpretation provided a simple, reliable, and well documented method for deriving fuel classification polygons on orthomosaic imagery from a UAS. It is easily replicated not only with UAS imagery but can also be used with satellite imagery or even NAIP if temporal scale is not an issue. Using this method provides land managers an easy way to classify fuels of their units and oftentimes it is these land managers who know their land and what fuels classification an area may represent. A shortcoming of this approach is potentially the need to provide realistic and specific fuel properties for fuels of each type of polygon. They could be estimated from field measurements like what was done in this thesis, or they could be estimated from other measurement and modeling systems such as fire behavior fuel models or the Fuel Characteristics Classification System (FCCS) that summarize fuel attributes as a function of fuel or forest type. Either way, there is a potentially time-consuming step to attribute polygons with realistic fuels data. The polygon approach is well suited to the STANDFIRE-to-FIRE-MODEL pathway because STANDFIRE incorporates the logic to distribute fuels within polygons based on estimates of cover, height, and patch size,

among other metrics. Using automated techniques may also provide another avenue for reliable fuels classifications such as a supervised classification of principal components as shown in figure 26 (C. Moran, 2020, unpublished) for Brattain Plot H, which closely matches the image interpretation technique mentioned earlier. Other techniques such as convolutional neural networks and Random Forests could also be explored to train an automated classification algorithm on high resolution UAS imagery (Duarte, Andriolo et al. 2020). Using spectral differences in addition to height data could also prove to be a fruitful avenue of investigation regarding automatic image classification as was mentioned in section 3.3 where multispectral images were used for confirming what was a shrub based on reflectivity in the NIR.

## 4.2 Objective 2. Attribute Fuel Polygons from Field Measurements

Attributing the fuel polygons, although simple in practice, proved challenging with the number of samples taken in the plots, variable location control, and lack of systematic, unbiased sampling in all the fuel types. In 2019, methods were improved with the use of the overhead aerial photos being used to guide the sampling strategy. The application of a high-accuracy differential GPS to locate field plots also

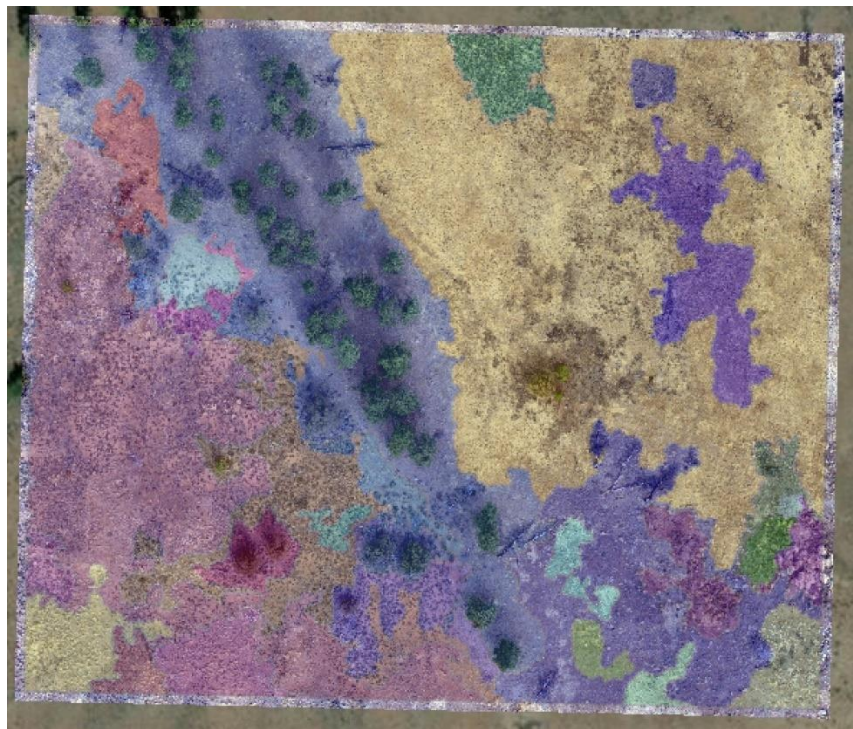


*Figure 18. Segmentation fuel classification based on principle component analysis*

*(C. Moran, 2020, unpublished)*

improved the quality of results. Despite shortcomings, this approach provided a simple framework on how to attribute imagery for use in fire modeling, and with a more robust sampling method, other plots could easily be sampled and attributed in better fashion. A more systematic sampling method would have greatly improved the attribute data, particularly in 2018, but as shown in earlier methods, there are ways to improve or gather sampling data after the imagery has been processed using conventional dot grids and perhaps directly from the CHM with a bit more research. In 2017, the intent was to use a pixel-based classification using orange CDs to locate areas sampled but due to inaccurate locations and poor-resolving power in the imagery, this approach was later switched to the current approach of using polygon-based units. The primary benefit of a pixel-based approach is the potential ability to link height and spectral data from the point cloud directly to specific fuel attributes such as bunch grass, coarse wood, or shrub. Another approach is to use object-based identification as was explored in section 3.3 above for shrub dimensions. This approach could be useful for identifying objects such as shrubs but would still not account for other fuels such as litter or grasses that are not object-based fuels. In the end, the simplicity of the polygon approach prevailed, and although it does not account for all the spatial variability, it does allow for the variability to be expressed correctly within polygons.

### **4.3 Objective 3. Quantify and Compare Shrub Heights and Widths**

The point clouds derived from imagery obtained at a height of 100m AGL (3cm Ground Sample Distance) underestimate the height of small, close-to-the-ground objects such as shrubs and overestimate their widths. One of the main areas of concern with respect to height is how to define ground so that an accurate canopy height model can be derived. Photo-derived point clouds only



produce points where matter is visible, often missing low points in shadows and between objects. The method of assuming that minimum heights within a neighborhood are ground is logical, but there was not a good way to verify the quality of the bare earth model in this study. The overestimation of shrub widths is in part attributable to the edge problem where pixels with specific dimensions encompass only a part of the shrub and artificially extend its edge outward. However, pixel-size was 3cm, so there is probably something else going on too. Distinguishing ground at the edge of objects such as trees (and shrubs) is difficult because the ground tends to be noisy where the algorithms can't determine whether a point is on the object or in the background. This effect may also be contributing to the artificial widening of shrubs in the CHM. In the end, shrub, and shrub-like objects (rocks) are reliably identifiable in the CHM but they produce fuel beds that are shorter and have higher cover than reality. Another issue with CHM derived shrub cover is that it also includes other objects such as coarse woody debris (CWD) which will artificially inflate shrub cover by incorporating it into the estimates. It seems possible that this issue could be overcome by incorporating spectral data in a classification in addition to height data.

#### **4.4 Objective 4. Assess Shrub Cover Derived from UAS Point Clouds**

Automated extraction of shrub cover from the CHM was compromised by many of the issues discussed in Section 3, above. After experimenting with many resolutions, height thresholds, and filters, the best results severely underestimated actual shrub cover for two primary reasons. First, the edges of shrubs either were too conservative or filled in all the space between shrubs at different settings without anything in between. Second, small diameter shrubs were consistently missed by the method. The idea still seems promising with a better CHM, and a more

conventional classification or machine learning approach that utilizes the height data along with spectral information from the optical band passes could be useful. Although not entirely conclusive, the results from the dot-grid suggest that the information content for shrub cover is contained in the ortho-imagery, and it is interesting that such an old-fashioned approach produced the best result. The results could potentially be improved when using multispectral data during a different season. In this case, data were collected at the very end of the growing season so much of the spectral information that the shrubs could have exhibited due to photosynthesis had ceased. However, it does require interpretation by a person and these types of methods have mostly fallen out of favor in modern science where automation is preferred. Another area of improvement to help identify smaller shrubs could be to use a higher resolution camera but with higher resolutions come larger datasets which greatly increases the already long processing times and when using modeling to run almost real-time fire behavior this would become an issue. Another issue with using the CHM derived shrub cover is based on how the SfM software reconstructs the shrubs which suffer greatly from any defined geometry whereas objects with very defined geometry are often reconstructed much better utilizing the algorithms based in the software. SfM suffers greatly when objects lack any defined geometry due to lack of initial tie points when reconstructing the objects from photos. Others approaches for imaging surface fuels have been shown to improve the quality of the reconstruction but rely on flying under the canopy manually which is very difficult and time consuming and defeats the purpose of an autonomous data collection.

## 4.5 Data Collection and Data Quality

Quality data matching the objectives of users is the most important factor to consider when collecting UAS data. One of the main issues with UAS data in forests is shadows and the effect of shadows in the reconstruction of 3D space. There are several papers and workflows published on methods to alleviate the issues associated with shadows (e.g., Rahman, McDermid et al. 2019) but these often require techniques to “fill-in” data in the areas where there is no information, or they are unreliable and time consuming to collect considering the workflows needed to blend imagery from different illumination conditions. Fortunately, this project was not strongly affected by shadows because some of the best collection days for forest plots happened when there was a large wildfire nearby that blocked the sun and created ideal diffuse lighting conditions with zero shadow effects (2018). Then in 2019, most of the study plots were grass rather than forest, in these areas, the shadows from shrubs and grasses appeared to increase texture and contrast and perhaps add information content to the images.

One of the biggest issues in processing was deriving a valid ground model from the 3D point cloud. Determining height variability from 3D point clouds was problematic due to the noise that remained from the 3D point cloud when information was lost along the edge of tree canopies where the algorithms have difficulty separating ground from crown. For grass fuel classes, it was impossible with the current camera configuration to get an accurate assessment of grass height due to the resolution of the pixel sampled being larger than the individual grass component. The same can be true for shrub fuel types that are leafless because the branches are often smaller resolution than the sensor is capable of sensing. Increasing resolution may solve this problem but it also increases the amount of processing time.

Due to the amount of time spent processing data, the computing power needed to process the data and steep learning curve as well as the constant “beta” testing of UAS hardware and software it may be more economical for land managers to use satellite-based imagery for fuel surveys of this type, particularly for those based on polygons and gradients. Satellite-based image resolution is increasing, as is its availability, coverage, and temporal frequency.

Additionally, anecdotal evidence suggests that for every hour of data collection, there will be about ten hours spent processing the data, and there is not a single UAS system that can collect every data set needed. Rather, it often is necessary build the UAS around the data to be collected.

Finally, a more robust and systematic field sampling method would have greatly increased the efficacy of the fuel samples and in hindsight more samples should have been collected at each plot so they could have been attributed on per plot basis instead of on a unit basis. The overhead pictures in 2019 greatly increased the sampling accuracy by ensuring that data was collected across the full range of variability seen within the images.

## 5. Conclusions

The primary intent of this project was to produce useful inputs to the STANDFIRE fuels translator to prepare fuels data for use in physics-based fire models. Fuel type polygons were effectively and efficiently delineated using traditional photo-interpretation. Each fuel polygon was attributed from field-collected data based on its dominant fuel type represented within that polygon. Differences between fuel type polygons were assessed statistically to document the distinctiveness of each fuel type, to overcome field sample-size limitations, and to provide logic

for merging fuel types that were similar in 2018. Plots in 2019 were also assessed statistically to document the distinctiveness of each fuel type and to assess the difference among plots.

Although these methods were done on a smaller scale this workflow is easily repeatable for large areas such as for a burn unit instead of on a plot scale.

The secondary intent of this project was to examine 3D point clouds and orthomosaics to better understand their information content for more detailed characterizations of fuels. Shrub height, width, and cover were extracted from the point clouds and compared to field measurements. The findings showed that fuel type classes were easily delineated using photo-interpretation, and effective attribution of fuel polygons was dependent on how and where field data were collected and differed by year. Lack of sufficient sample sizes in some fuel type polygons required aggregation of field data from all plots within the Brattain burn unit in 2018. These shortcomings were overcome in 2019 by acquiring rapid-look imagery prior to field sampling that enabled more balanced samples across the range of variability observed within the rapid-look imagery. Within the point-clouds, shrub height was underestimated while width was over-estimated. Shrub cover was also under-predicted from the point cloud and was better enumerated using a conventional dot-grid approach on the orthomosaic. Although shrub height was over estimated and shrub width was underestimated the 3D point clouds did provide some height and width information just not the same measurements as taken in the field. If these over and under estimations remain constant across other datasets it could prove that by just adjusting the height and width by a constant value could improve the value of height and width information within the 3D point clouds. Shrub cover could also possibly be improved with higher resolution imagery and a smaller GSD, this can be achieved by either increasing the camera resolution or decreasing the height the imagery was collected at. Improvements in data collection methods and

technology from 2017-2019 have resulted in a stable workflow that produces consistent fuels data formatted for STANDFIRE. The polygon-based approach is suitable for use in fire model validation due to its ability to rationally capture and integrate sparse field data because STANDFIRE is designed to work easily with polygons, and because there is insufficient evidence that model validation is at a point where it will benefit from use of more complex pixel or object-based inputs. Automated approaches to polygon delineation via region-growing, machine learning, and segmentation are a logical next step with the caveat that the inputs derived in this study should be tested in the modeling environment first. After validating that these fuel polygons are accurate and what fire behavior models need, AI based on-the-fly classification could possibly be another logical step in classifying surface fuels. Given the steep learning curve to collect proper actionable UAS data, expensive hardware, and software it may be easier and more economical to use other high-resolution imagery available if temporal scale is not an issue. These other sources could be NAIP or satellite imagery.

## 6. References Cited

Avery, T. E. (1966). Forester's guide to aerial photo interpretation, US Department of Agriculture, Forest Service.

Bhandari, B., U. Oli, et al. (2015). Generation of high resolution DSM using UAV images. FIG Working Week.

Bradshaw, J. C. B. (1986). Fire behavior modeling-a decision tool. Prescribed Burning in the Midwest: State of the Art Symposium. Stevens Point, Wisconsin, Fire Management Today. **66**.

Calkin, D. E., J. D. Cohen, et al. (2014). "How risk management can prevent future wildfire disasters in the wildland-urban interface." Proceedings of the National Academy of Sciences **111**(2): 746-751.

Canis, B. (2015). Unmanned aircraft systems (UAS): Commercial outlook for a new industry, Congressional Research Service Washington, DC.

Carrivick, J., M. Smith, et al. (2016). Structure from motion in the geosciences. Chichester, West Sussex, UK ; Ames, Iowa, John Wiley & Sons, Inc.

Çelik, M. Ö., A. Alptekin, et al. (2020). "The Effect of Different Flight Heights on Generated Digital Products: Dsm And Orthophoto." J Mersin Photogrammetry Journal **2**(1): 1-9.

Cleaves, D. A., T. K. Haines, et al. (1999). Prescribed burning costs: trends and influences in the National Forest System. Proc. of the Symposium on fire economics, planning, and policy: Bottom lines, USDA For. Serv., Gen. Tech. Rep. PSW-GTR-173, Pacific Southwest Research ....

Crookston, N. and G. Dixon (2005). "The forest vegetation simulator: A review of its structure, content, and applications." Comput. Electron. Agric. **49**(1): 60-80.

FAR/AIM (2016). Aeronautical Information Manual/Federal Aviation Regulations, McGraw-Hill.

Guo, F., Y. Ji, et al. (2001). "Methods for improving the accuracy and reliability of vehicle-borne GPS intelligence navigation."

Han, S. and C.-K. Hong (2019). "Assessment of parallel computing performance of Agisoft Metashape for orthomosaic generation." Journal of the Korean Society of Surveying, Geodesy, Photogrammetry

Cartography **37**(6): 427-434.

James, K. B. (1970). "Ratios of Surface Area to Volume For Common Fine Fuels " Forest Science **16**: 101-105.

James, M. R., S. Robson, et al. (2017). "Optimising UAV topographic surveys processed with structure-from-motion: Ground control quality, quantity and bundle adjustment." Geomorphology **280**: 51-66.

Keane, R. E., L. J. Dickinson, et al. (2007). The photoload sampling technique estimating surface fuel loadings from downward-looking photographs of synthetic fuelbeds. General technical report RMRS GTR-190. Fort Collins, CO, U.S. Dept. of Agriculture, Forest Service, Rocky Mountain Research Station, 44 pages.

Kolden, C. A. (2019). "We're not doing enough prescribed fire in the western United States to mitigate wildfire risk." Fire **2**(2): 30.

Lillesand, T. M., R. W. Kiefer, et al. (2008). Remote sensing and image interpretation.

Linn, R. R., S. L. Goodrick, et al. (2020). "QUIC-fire: A fast-running simulation tool for prescribed fire planning." Environmental Modelling & Software **125**: 104616.

McGrattan, K., R. McDermott, et al. (2012). "Computational fluid dynamics modelling of fire." International Journal Computational Fluid Dynamics **26**(6-8): 349-361.

McGrattan, K. B. and T. National Institute of Standards and (2000). Fire dynamics simulator technical reference guide. Gaithersburg, MD, Gaithersburg, MD : U.S. Dept. of Commerce, Technology Administration, National Institute of Standards and Technology.

Mell, W., J. Charney, et al. (2013). Numerical simulations of grassland fire behavior from the LANL-FIRETEC and NIST-WFDS models. Remote Sensing and Modeling Applications to Wildland Fires, Springer: 209-225.

Mell, W., M. A. Jenkins, et al. (2007). "A physics-based approach to modelling grassland fires." Int. J. Wildland Fire **16**(1): 1-22.

Merry, K. and P. Bettinger (2019). "Smartphone GPS accuracy study in an urban environment." PLOS ONE **14**(7): e0219890.

Moran, C., J. , C. Seielstad, A. , et al. (2019). "Deriving Fire Behavior Metrics from UAS Imagery." Fire **2**(2): 36.

Ng, K. M., J. Johari, et al. (2018). Performance Evaluation of the RTK-GNSS Navigating under Different Landscape. 2018 18th International Conference on Control, Automation and Systems (ICCAS).



Noonan-Wright, E. K., N. M. Vaillant, et al. (2014). "The effectiveness and limitations of fuel modeling using the Fire and Fuels Extension to the Forest Vegetation Simulator." Forest Science **60**(2): 231-240.

Paine, D. P. and J. D. Kiser (2012). Aerial photography and image interpretation, John Wiley & Sons.

Park, H. M. J. I. U. (2009). "Comparing group means: t-tests and one-way ANOVA using Stata, SAS, R, and SPSS."

Patrick, S., S. Temuulen, et al. (2018). "Evaluating Unmanned Aerial Vehicle Images for Estimating Forest Canopy Fuels in a Ponderosa Pine Stand." Remote Sensing **10**(8): 1266.

Pimont, F., R. Parsons, et al. (2016). "Modeling fuels and fire effects in 3D: Model description and applications." Environmental Modelling & Software **80**(C): 225-244.

Prichard, S., B. Keane, et al. (2017). "Hierarchical 3D fuel and consumption maps to support physics-based fire modeling." Joint Fire Science Program.

Radeloff, V. C., D. P. Helmers, et al. (2018). "Rapid growth of the US wildland-urban interface raises wildfire risk." Proceedings of the National Academy of Sciences **115**(13): 3314-3319.

Rahman, M. M., G. J. McDermid, et al. (2019). "A workflow to minimize shadows in UAV-based orthomosaics." Journal of Unmanned Vehicle Systems **7**(2): 107-117.

Reinhardt, E. D. (2003). The fire and fuels extension to the forest vegetation simulator, United States Department of Agriculture, Forest Service, Rocky Mountain ....

The Nature Conservancy (2020). "Sycan Marsh Preserve." from <https://www.nature.org/en-us/get-involved/how-to-help/places-we-protect/sycan-marsh/>.

Tripcevich, N. (2017). "Developments in Archaeological Field Recording." [escholarship.org](http://escholarship.org).

U.S. Climate Data (2020). "Climate Silver Lake - Oregon." from <https://www.usclimatedata.com/climate/silver-lake/oregon/united-states/usor0322>.

Duarte, D., et al. (2020). "Addressing the class imbalance problem in the automatic image classification of coastal litter from orthophotos derived from uas imagery." **3**: 439-445.

Hanson, H. P., et al. (2000). "The potential and promise of physics-based wildfire simulation." **3**(4): 161-172.

Hoffman, C. M., et al. (2018). "Advancing the science of wildland fire dynamics using process-based models." **1**(2): 32.

Meerpoel-Pietri, K., et al. (2022). "Modeling with WFDS Combustion Dynamics of Ornamental Vegetation Structures at WUI: Focus on the Burning of a Hedge at Laboratory Scale." 1-31.

Ottmar, R. D., et al. (2007). "An overview of the fuel characteristic classification system—quantifying, classifying, and creating fuelbeds for resource planning." **37**(12): 2383-2393.

Young, J. D., et al. (2020). "Effects of policy change on wildland fire management strategies: evidence for a paradigm shift in the western US?" **29**(10): 857-877.

# 7. Appendices

## 7.1 Appendix A

Below is an output of a text file from STANDFIRE.

# Default additional properties file

HT= Height, PD= Particle density, BD= Bulk Density, PS=Patch Size

understoreyFuelOption=1

```

{(1,1);(191,1);(191,127);(1,127)}          {(191,0);(192,0);(192,128);(191,128)}
  {1;2} {false;false}                        {7;8} {false;false}
{(0,0);(1,0);(1,128);(0,128)}              {(1,0);(191,0);(191,1);(1,1)}
  {3;4} {false;false}                        {9;10} {false;false}
{(1,127);(191,127);(191,128);(1,128)}      {(0,0);(192,0);(192,128);(0,128)}
  {5;6} {false;false}                        {11} {true}
  Height Base HT Cover PS                    7   Shrub 0.35  0.0  0.5  5.0
1   Shrub 0.35  0.0  0.5  5.0                1
  1                                           Leave_Live 0.72  500  5000  100
Leave_Live 0.72BD      500PD                Leave_Dead 0.08  500  5000  40
  5000SAV      100Moisture                8   Herb 0.35  0.0  0.8  1.0
Leave_Dead 0.08  500  5000  40              1
2   Herb 0.35  0.0  0.8  1.0                Leave_Live 0.0  500  5000  100
  1                                           Leave_Dead 0.8  500  5000  5
Leave_Live 0.0BD 500PD 5000SAV              9   Shrub 0.35  0.0  0.5  5.0
  100Moisture                                1
Leave_Dead 0.8  500  5000  5                Leave_Live 0.72  500  5000  100
3   Shrub 0.35  0.0  0.5  5.0                Leave_Dead 0.08  500  5000  40
  1                                           10  Herb 0.35  0.0  0.8  1.0
Leave_Live 0.72  500  5000  100              1
Leave_Dead 0.08  500  5000  40                Leave_Live 0.0  500  5000  100
4   Herb 0.35  0.0  0.8  1.0                Leave_Dead 0.8  500  5000  5
  1                                           11  Litter 0.1  0.0  1.0  -1.0
Leave_Live 0.0  500  5000  100              0
Leave_Dead 0.8  500  5000  5                Litter 0.5  500  2000  10
5   Shrub 0.35  0.0  0.5  5.0                DefaultLeave_Live 0.9  150
  1                                           DefaultTwig1_Live 0.9  100
Leave_Live 0.72  500  5000  100              DefaultTwig2_Live 0.9  80
Leave_Dead 0.08  500  5000  40              DefaultTwig3_Live 0.9  70
6   Herb 0.35  0.0  0.8  1.0                DefaultLeave_Dead 0.1  10
  1                                           DefaultTwig1_Dead 0.1  10
Leave_Live 0.0  500  5000  100              DefaultTwig2_Dead 0.1  10
Leave_Dead 0.8  500  5000  5                DefaultTwig3_Dead 0.1  10
PSME Leave_Live 0.9  150

```

PSME Twig1_Live	0.9	100	PSME Twig1_Dead	0.1	10
PSME Twig2_Live	0.9	80	PSME Twig2_Dead	0.1	10
PSME Twig3_Live	0.9	70	PSME Twig3_Dead	0.1	10
PSME Leave_Dead	0.1	10			

## 7.2 Appendix B

### ArcGIS Shapefile Key

Fuel Type – from dominant fuel in imagery for each polygon

sh\_ht – average height of shrub from field plots (m)

sh\_base – base height of shrub, assumed 0 (m)

sh\_cover – average shrub cover from field plots (percent)

**sh\_patch – average shrub diameter from field plot subset (used for all droneplots) (m)**

sh\_intcode – code from STANDFIRE (check with russ on meaning) (integer)

**sh\_live\_bd – constant – used STANDFIRE example – no load data from field (kg/m<sup>3</sup>)**

sh\_live\_pd – particle density constant – used STANDFIRE example (kg/m<sup>3</sup>)

sh\_livesav – live surface area to volume constant – used STANDFIRE example (m<sup>-1</sup>)

sh\_liveh2o – live moisture constant – used STANDFIRE example (adjust from field) (percent)

sh\_dead\_bd – dead bulk density – used STANDFIRE example, no data on live vs dead (kg/m<sup>3</sup>)

sh\_dead\_pd – dead particle density constant used – used STANDFIRE example (kg/m<sup>3</sup>)

sh\_deadsav – dead surface area to volume constant – used STANDFIRE example (m<sup>-1</sup>)

sh\_deadh2o – dead moisture constant – used STANDFIRE example (adjust from field) (percent)

hb\_ht – average height of herb from field plots (m)

hb\_base – base height of herb, assumed 0 (m)

hb\_cover – average herb cover from field plots (percent)

**hb\_patch – average herb patch size constant (1) – used STANDFIRE example (m)**

hb\_intcode – code from STANDFIRE (check with russ on meaning) (integer)

hb\_live\_bd – average live bulk density set to 0 (all herb assumed dead) (kg/m<sup>3</sup>)

hb\_live\_pd – live particle density constant – used STANDFIRE example (kg/m<sup>3</sup>)

hb\_livesav – live surface area to volume constant – used STANDFIRE example (m<sup>-1</sup>)

hb\_liveh2o – live moisture constant – used STANDFIRE example (adjust from field) (percent)

hb\_dead\_bd – dead bulk density – used STANDFIRE example, no data on live vs dead (kg/m<sup>3</sup>)

**hb\_dead\_pd – average dead particle density, calculated from height and load from field plots (kg/m<sup>3</sup>)**

hb\_deadsav – dead surface area to volume constant – used STANDFIRE example (m<sup>-1</sup>)

hb\_deadh2o – dead moisture constant – used STANDFIRE example (adjust from field) (percent)

lit\_ht – average thickness (depth) of litter layer from field plots (m)

lit\_base – 0 (m)

lit\_cov – average litter cover from field plots (percent)

**lit\_patch - litter patch size constant (-1) – used STANDFIRE flag (-1) example (m)**

lit\_intcode – code from STANDFIRE (check with russ on meaning) (integer)

lit\_bd – litter bulk density constant – used STANDFIRE example, no field load data for litter (kg/m<sup>3</sup>)

lit\_pd – litter particle density constant – used STANDFIRE example

lit\_sav – litter surface area to volume constant – used STANDFIRE example (m<sup>-1</sup>)

lit\_h2o – litter moisture constant – used STANDFIRE example (adjust from field) (percent)

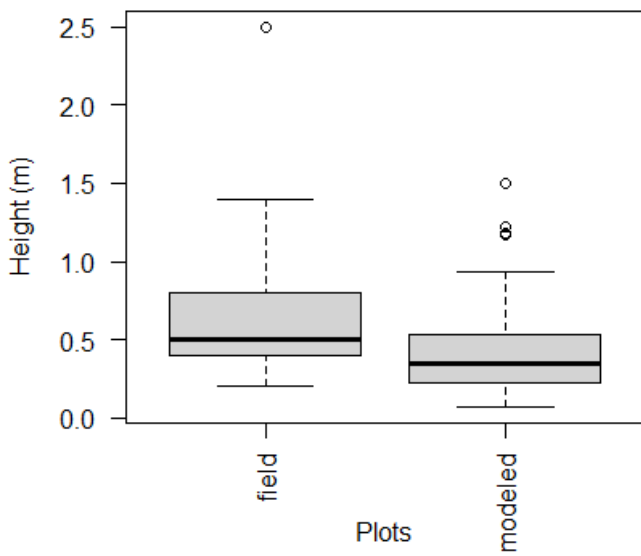
## 7.3 Appendix C

### Charts and plots

Plot	Year	Burn Unit	Sensor
Brattain_B	2018	Brattain	X3/MSRE
Brattain_C	2018	Brattain	X3/MSRE
Brattain_F	2018	Brattain	X3/MSRE
Brattain_H	2018	Brattain	X3/MSRE
1A_Grass	2019	BICO West	X3/MSRE
1C_Grass	2019	BICO West	X3/MSRE
1C_Forest	2019	BICO West	X3/MSRE
Southern_Grass_1	2019	BICO West	X3/MSRE
Southern_Grass_2	2019	BICO West	X3/MSRE
X3 – DJI Zemuse X3 12MP			
MSRE – Micasense Rededge Multispectral camera.			

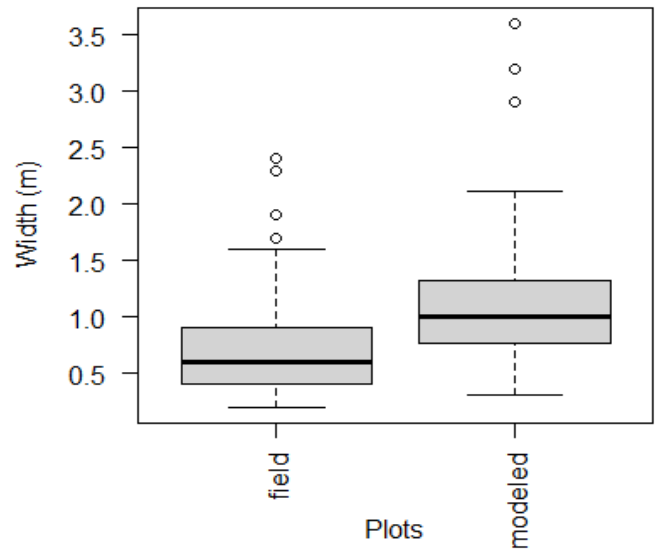
Plots used in this thesis.

**Modeled vs. Field Measured Shrub height**



Modeled Vs. Field Measured Shrubs Height.

**Modeled vs. Field Measured Shrub width**



Modeled Vs. Field Measured Shrubs width.

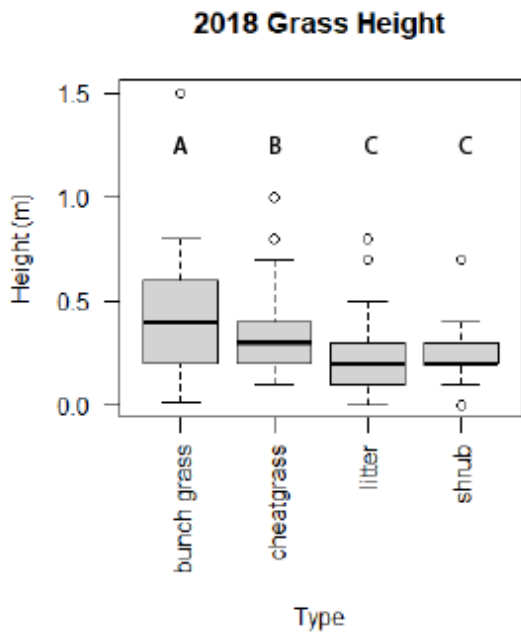
Plot	Fuel Class	N	Percent Cover	SD	Median	Min	Max	Range	Skewness	Kurtosis	SE
Brat H	Cheat Grass	25	49	27.08	38	13	88	75	0.24	-1.32	5.42
Brat H	Bunch Grass	0	n/a	n/a	n/a	n/a	n/a	n/a	n/a	n/a	n/a
Brat H	Litter	15	53	33.81	63	13	88	75	-0.12	-1.88	8.73
Brat H	Shrub	18	3.06	9.26	0	0	35	35	2.59	5.51	2.18
Brat G	Cheat Grass	0	n/a	n/a	n/a	n/a	n/a	n/a	n/a	n/a	n/a
Brat G	Bunch Grass	9	15.78	8.33	13	13	38	25	2.07	2.63	2.78
Brat G	Litter	26	53.38	33.22	50.5	13	88	75	-0.09	-1.56	6.52
Brat G	Shrub	10	0.5	1.58	0	0	5	5	2.28	3.57	0.5
Brat F	Cheat Grass	29	56.1	26.64	63	13	88	75	-0.49	-1.06	4.95
Brat F	Bunch Grass	39	39.9	29.36	38	0	88	88	0.36	-1.36	4.7
Brat F	Litter	6	2.17	5.31	0	0	13	13	1.36	-0.08	2.17
Brat F	Shrub	0	n/a	n/a	n/a	n/a	n/a	n/a	n/a	n/a	n/a
Brat E	Cheat Grass	0	n/a	n/a	n/a	n/a	n/a	n/a	n/a	n/a	n/a
Brat E	Bunch Grass	0	n/a	n/a	n/a	n/a	n/a	n/a	n/a	n/a	n/a
Brat E	Litter	9	51.89	33.33	63	13	88	75	-0.11	-1.92	11.11
Brat E	Shrub	6	0.83	2.04	0	0	5	5	1.36	-0.08	0.83
Brat D	Cheat Grass	0	n/a	n/a	n/a	n/a	n/a	n/a	n/a	n/a	n/a
Brat D	Bunch Grass	0	n/a	n/a	n/a	n/a	n/a	n/a	n/a	n/a	n/a
Brat D	Litter	0	n/a	n/a	n/a	n/a	n/a	n/a	n/a	n/a	n/a
Brat D	Shrub	1	0	n/a	n/a	n/a	n/a	n/a	n/a	n/a	n/a
Brat C	Cheat Grass	1	13	n/a	n/a	n/a	n/a	n/a	n/a	n/a	n/a
Brat C	Bunch Grass	0	n/a	n/a	n/a	n/a	n/a	n/a	n/a	n/a	n/a
Brat C	Litter	1	38	n/a	n/a	n/a	n/a	n/a	n/a	n/a	n/a
Brat C	Shrub	0	n/a	n/a	n/a	n/a	n/a	n/a	n/a	n/a	n/a
Brat B	Cheat Grass	5	44.25	37.5	38	13	88	75	0.14	-2.28	18.75
Brat B	Bunch Grass	0	n/a	n/a	n/a	n/a	n/a	n/a	n/a	n/a	n/a
Brat B	Litter	59	42.24	32.55	38	13	88	75	0.43	-1.6	4.24
Brat B	Shrub	0	n/a	n/a	n/a	n/a	n/a	n/a	n/a	n/a	n/a
Brat A	Cheat Grass	0	n/a	n/a	n/a	n/a	n/a	n/a	n/a	n/a	n/a
Brat A	Bunch Grass	2	25.5	17.68	25.5	13	38	25	0	-2.75	25
Brat A	Litter	37	37.32	28.56	38	13	88	75	0.7	-1.05	4.69
Brat A	Shrub	8	3.75	45.26	2.5	0	90	90	0.42	-2.02	16

2018 Brattain fuel sample statistics.

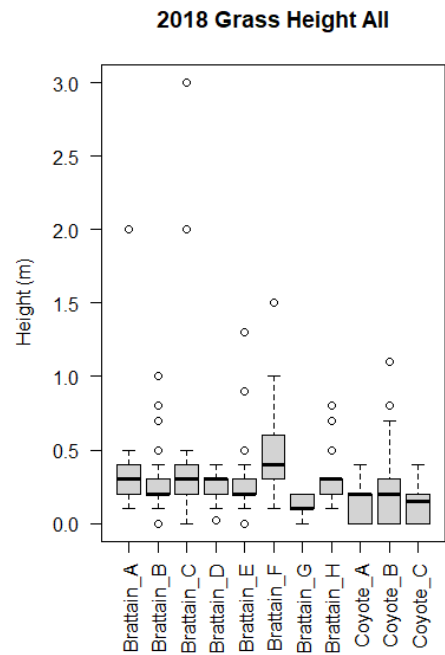


Plot	Fuel Class	N	Percent Cover	SD	Median	Min	Max	Range	Skewness	Kurtosis	SE
Forest_1C	Shrub	21	36.67	35.27	13	0	88	88	0.29	-1.69	7.7
Forest_1C	Bunch Grass	22	44.82	26.93	38	0	88	88	0.05	-1.23	5.74
Forest_1C	Litter	51	74.76	22.56	88	13	88	75	-1.52	1.09	3.16
Grass_1A	Shrub	0	n/a	n/a	n/a	n/a	n/a	n/a	n/a	n/a	n/a
Grass_1A	Bunch Grass	38	84.71	10.35	88	38	88	50	-3.12	9.45	1.68
Grass_1A	Litter	0	n/a	n/a	n/a	n/a	n/a	n/a	n/a	n/a	n/a
Grass_1C	Shrub	0	0	0	0	0	0	0	0	0	0
Grass_1C	Bunch Grass	50	70.5	20.98	75.5	13	75	62	-1	0.2	2.97
Grass_1C	Litter	0	n/a	n/a	n/a	n/a	n/a	n/a	n/a	n/a	n/a
1_SG	Shrub	0	n/a	n/a	n/a	n/a	n/a	n/a	n/a	n/a	n/a
1_SG	Grass	45	81.89	12.1	88	38	88	50	-1.72	2.08	1.8
1_SG	Litter	0	n/a	n/a	n/a	n/a	n/a	n/a	n/a	n/a	n/a
2_SG	Shrub	0	n/a	n/a	n/a	n/a	n/a	n/a	n/a	n/a	n/a
2_SG	Grass	39	84.15	9.14	88	63	88	25	-1.85	1.44	1.46
2_SG	Litter	0	n/a	n/a	n/a	n/a	n/a	n/a	n/a	n/a	n/a

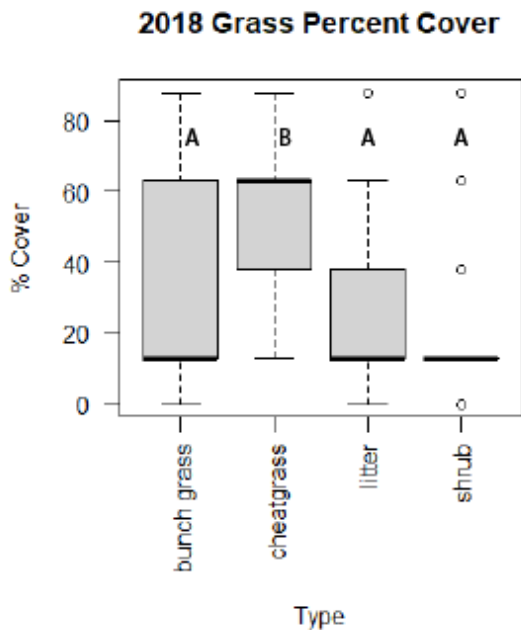
2019 BICO fuel sample statistics.



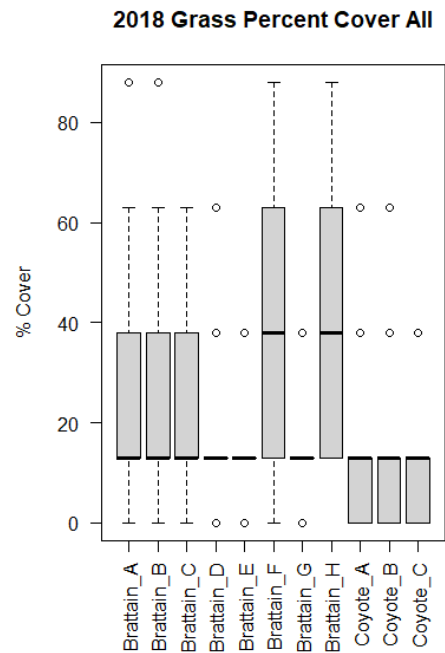
2018 grass height by fuel type. Differing letters above boxes denote statistically significant differences ( $p < 0.01$ ).



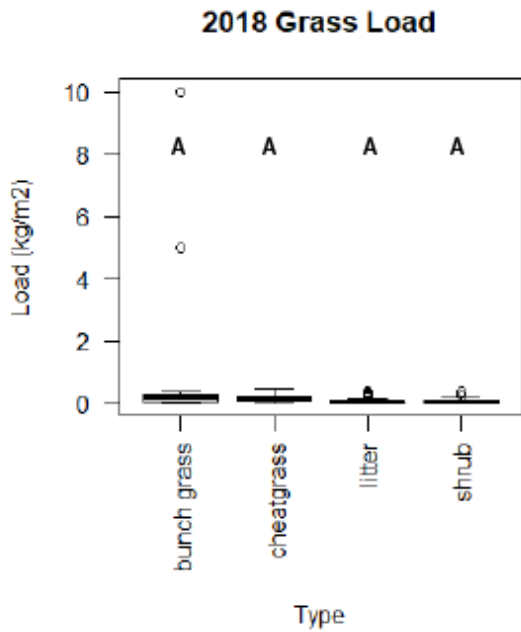
2018 all plots grass height.



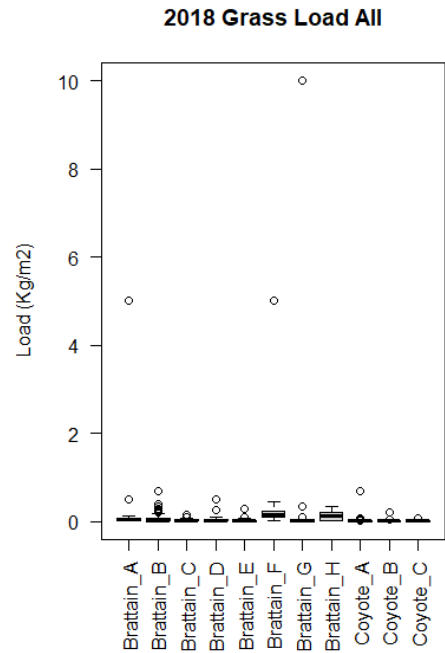
2018 grass cover by fuel type. Differing letters above boxes denote statistically significant differences ( $p < 0.01$ ).



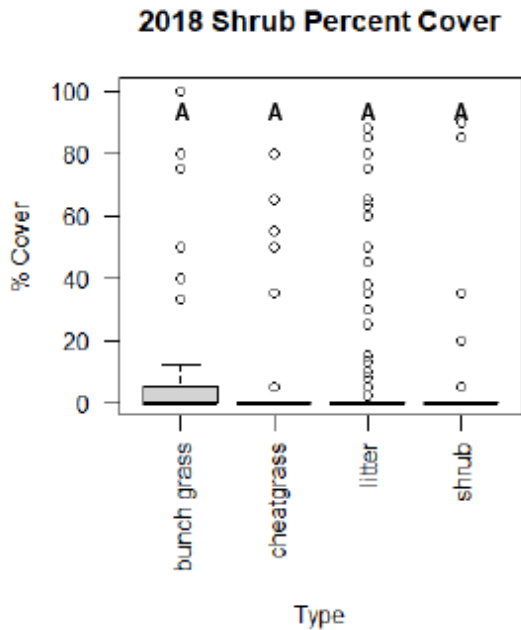
2018 all plots grass cover.



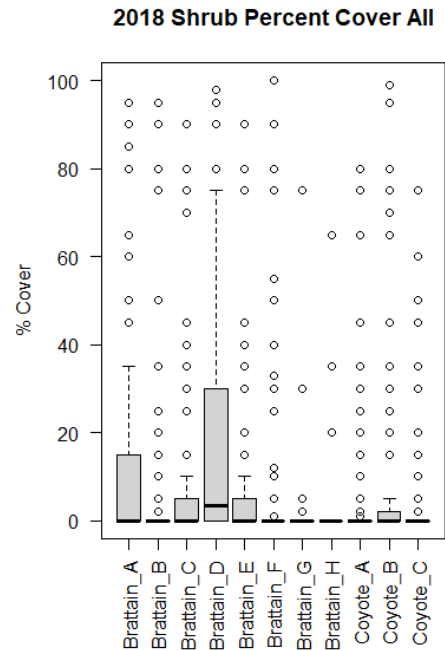
2018 grass cover by fuel type. Differing letters above boxes denote statistically significant differences ( $p < 0.01$ ).



2018 all plots grass cover.

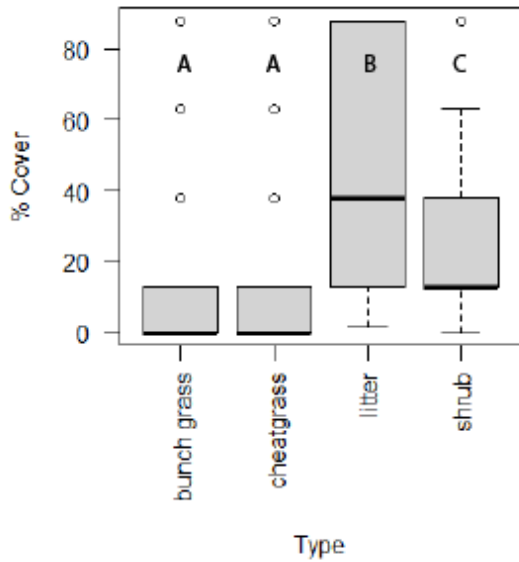


2018 shrub cover by fuel type. Differing letters above boxes denote statistically significant differences ( $p < 0.01$ ).



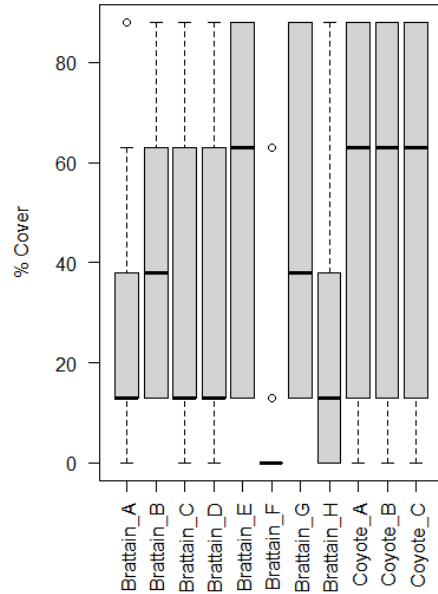
2018 all plots shrub cover.

**2018 Litter Percent Cover**



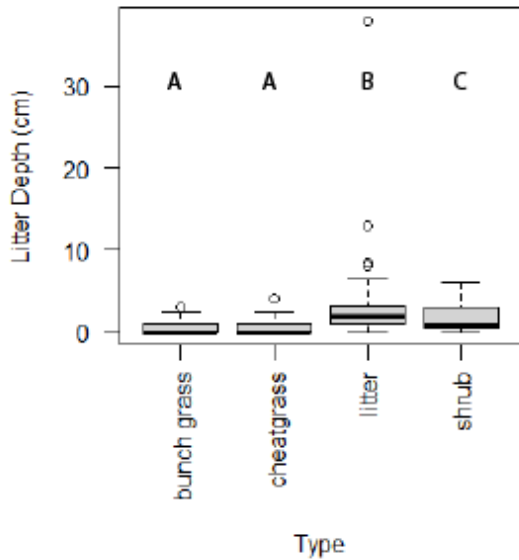
2018 litter cover by fuel type. Differing letters above boxes denote statistically significant differences ( $p < 0.01$ ).

**2018 Litter Percent Cover All**



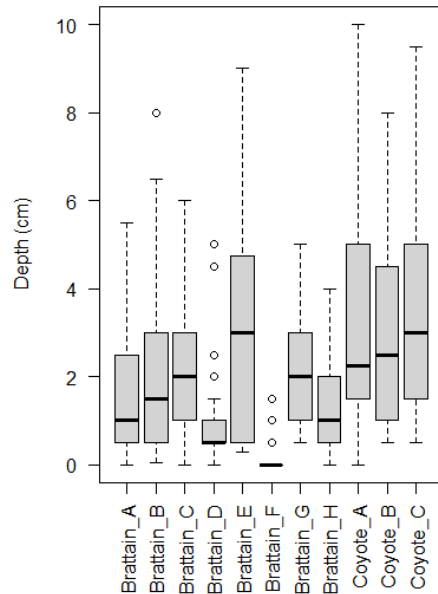
2018 all plots litter cover.

**2018 Litter Depth**

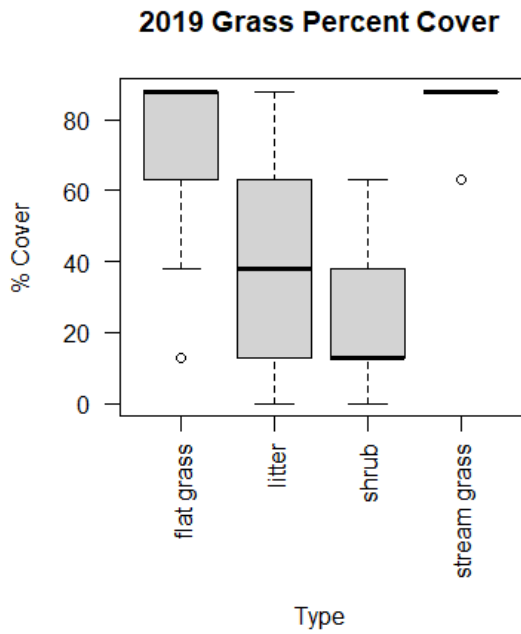


2018 litter depth by fuel type. Differing letters above boxes denote statistically significant differences ( $p < 0.01$ ).

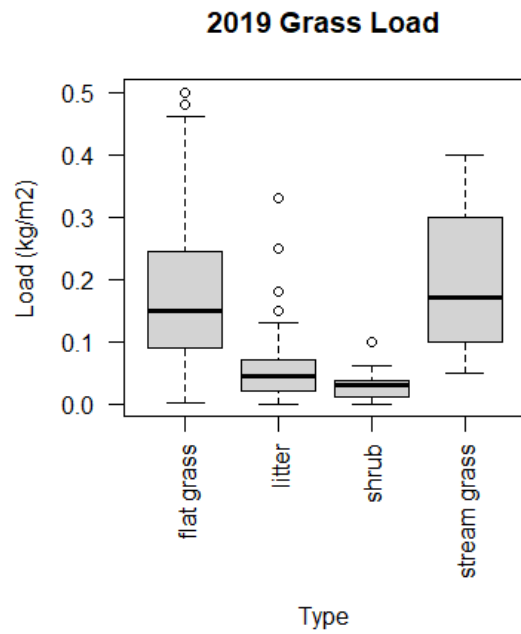
**2018 Litter Depth All**



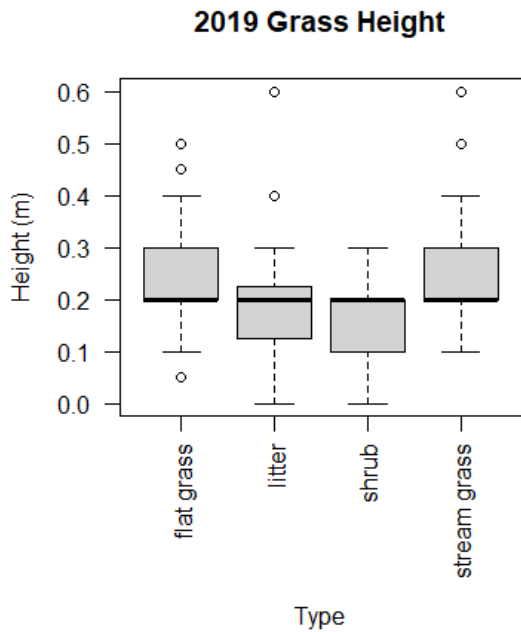
2018 all plots litter depth.



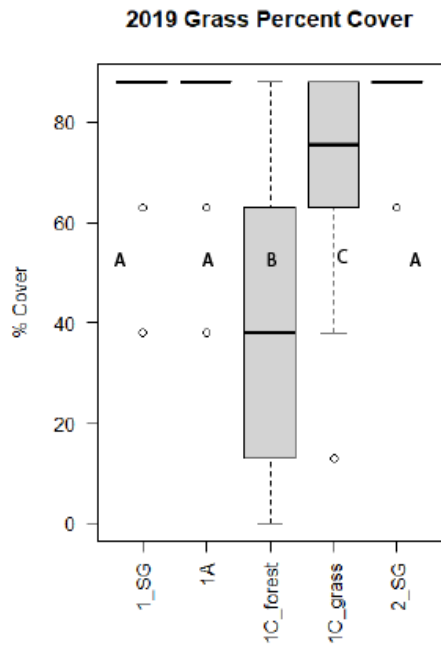
2019 grass cover by fuel type.



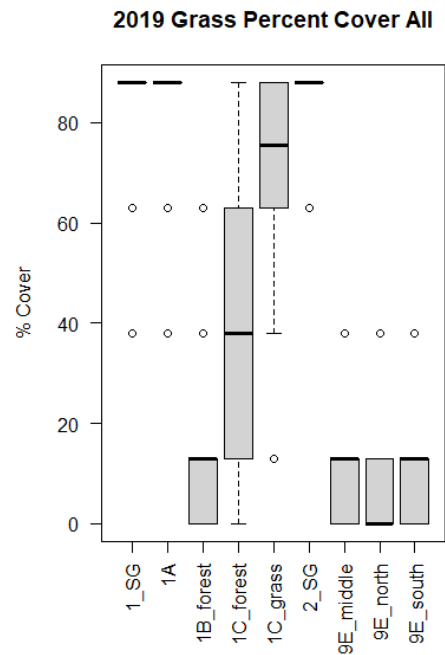
2019 grass load by fuel type.



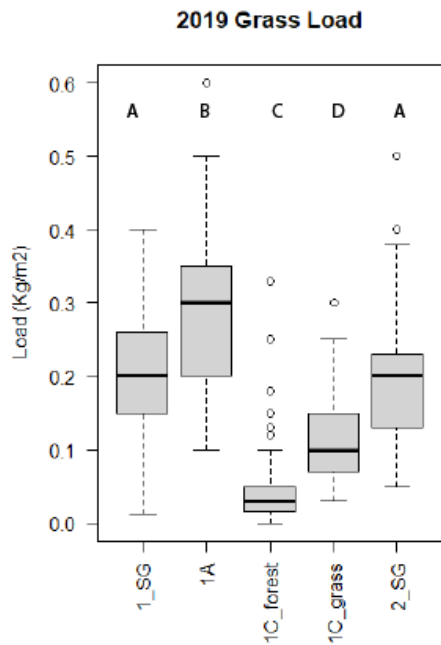
2019 grass height by fuel type.



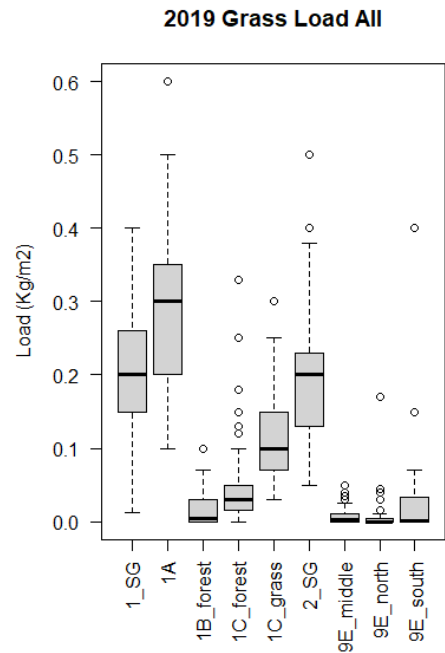
2019 grass cover by plot. Differing letters above boxes denote statistically significant differences ( $p < 0.01$ ).



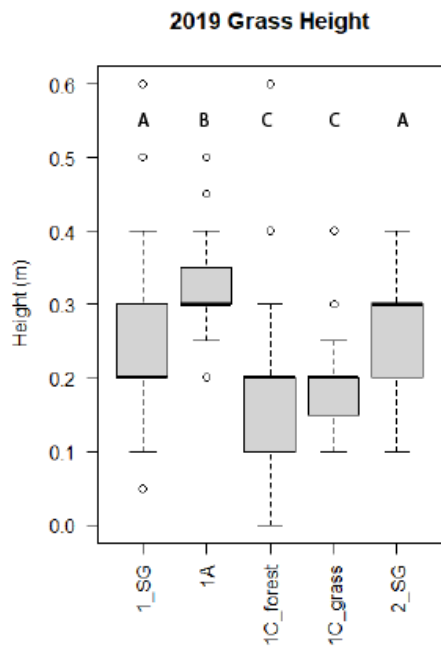
2019 all plots grass cover.



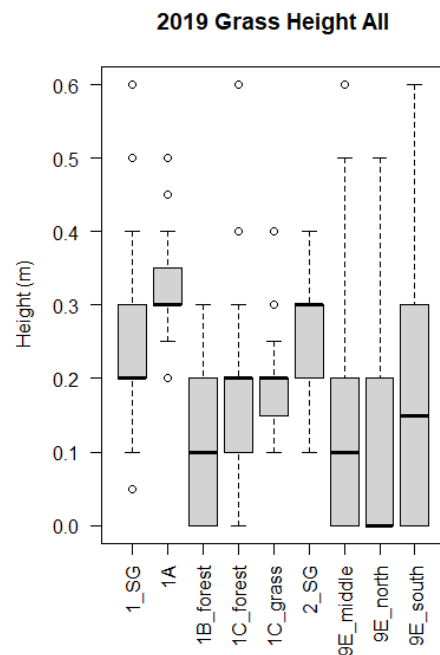
2019 grass load by plot. Differing letters above boxes denote statistically significant differences ( $p < 0.01$ ).



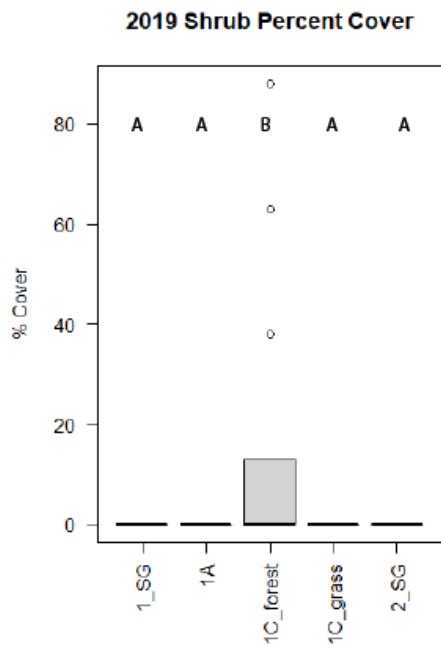
2019 all plots grass load.



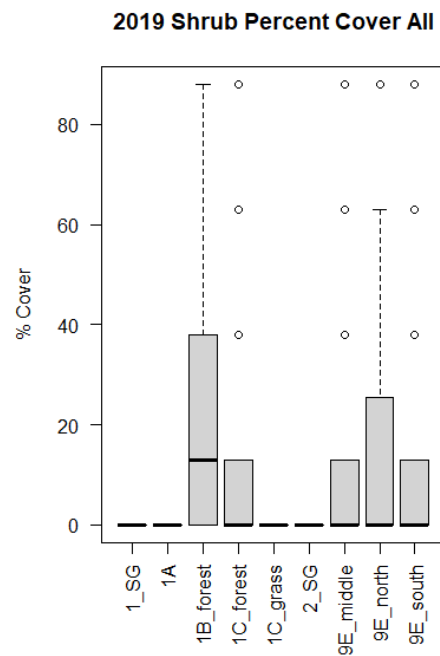
2019 grass height by plot. Differing letters above boxes denote statistically significant differences ( $p < 0.01$ ).



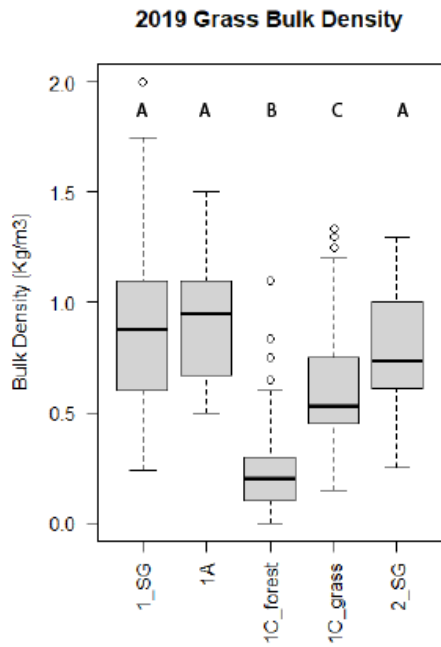
2019 all plots grass height.



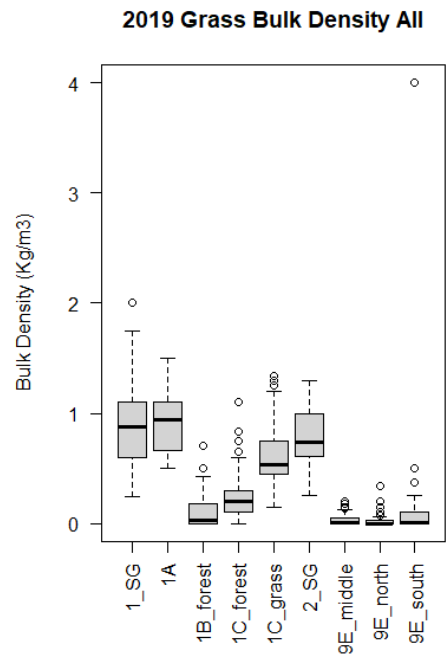
2019 shrub cover by plot. Differing letters above boxes denote statistically significant differences ( $p < 0.01$ ).



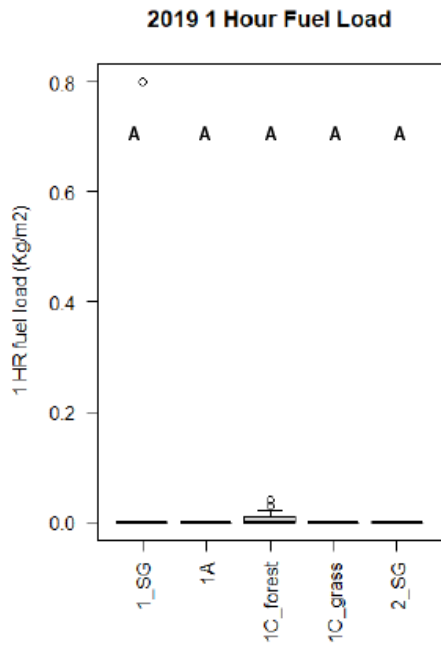
2019 all plots shrub cover.



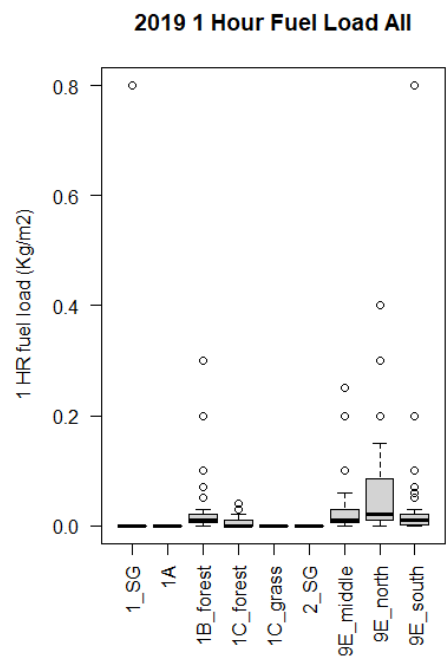
2019 grass bulk density by plot. Differing letters above boxes denote statistically significant differences ( $p < 0.01$ ).



2019 all plots grass bulk density.



2019 one-hour fuel by plot. Differing letters above boxes denote statistically significant differences ( $p < 0.01$ ).



2019 all plots one hour fuel load.



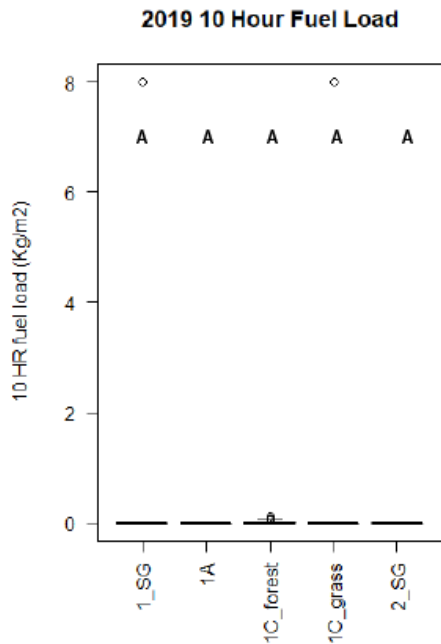
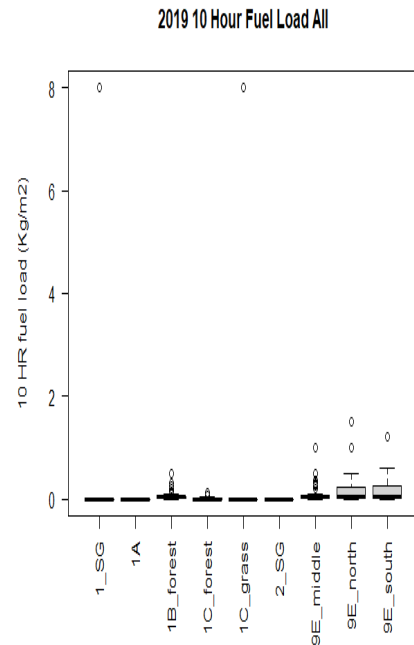
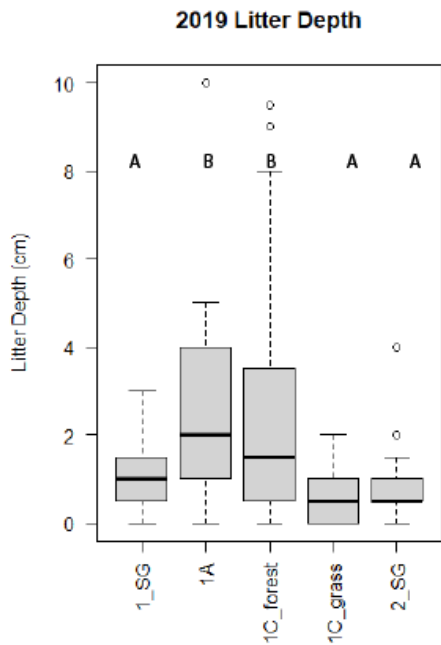


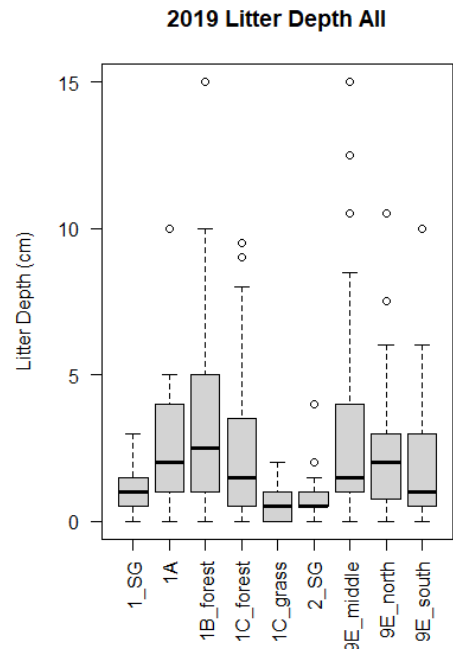
Figure 36. 2019 ten-hour fuel by plot. Differing letters above boxes denote statistically significant differences ( $p < 0.01$ ).



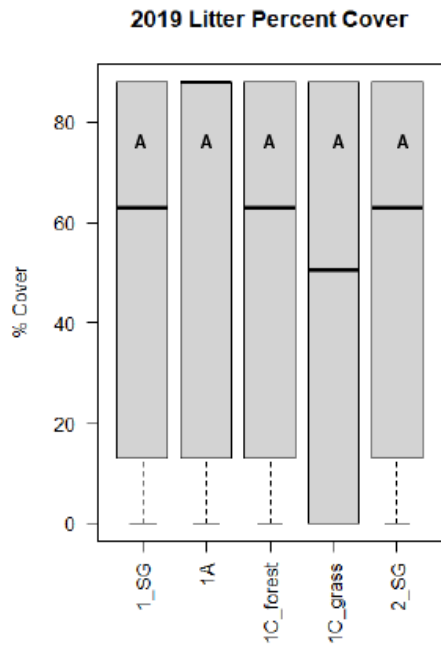
2019 all plots ten-hour fuel load.



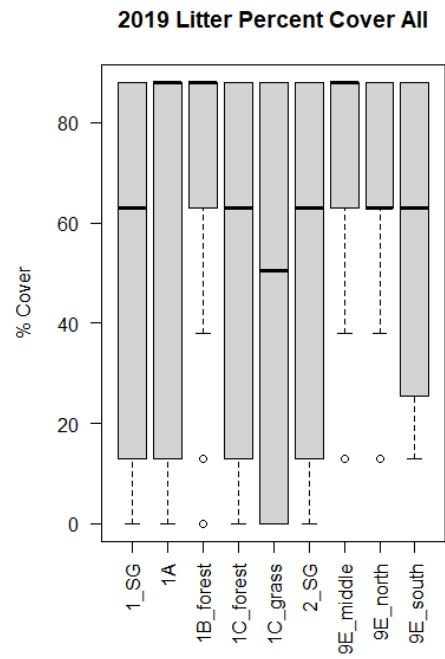
2019 Litter depth by plot. Differing letters above boxes denote statistically significant differences ( $p < 0.01$ ).



2019 all plots litter depth.



2019 Litter cover by plot. Differing letters above boxes denote statistically significant differences ( $p < 0.01$ ).



2019 all plots litter cover.